



Bubble curtains for noise mitigation: One vs two

Simon Beelen, ^{1,2,a)} Marten Nijhof, ³ Christ de Jong, ³ Leen van Wijngaarden, ¹ and Dominik Krug^{1,4,b)} Physics of Fluids Group and Max Planck Center for Complex Fluid Dynamics, J. M. Burgers Centre for Fluid Dynamics, University of Twente, P.O. Box 217, 7500AE, Enschede, The Netherlands

ABSTRACT:

Bubble curtains are widely used to protect marine life from exposure to harmful noise during offshore pile driving. However, operating a bubble curtain is costly and compliance with government noise regulations remains a challenge. It is therefore important to optimise the acoustic effect of the available compressed air. An interesting approach to achieving this is to split the air flow rate into two separate bubble curtains, rather than one single bubble curtain. This concept is tested both experimentally and numerically in this paper. The experiments and the model show the expected increase in performance of the supplied compressed air when it is split between two manifolds. An increased insertion loss of up to 11 dB is measured. This increase in performance is possibly due to the fact that the reflective properties of the bubble curtains are maintained even when the air flow rate is halved. In effect, by splitting the air flow between two manifolds, a second acoustic barrier is added. Additionally, the variations in the bubble curtain performance between individual measurements are shown to be largely caused by temporal variations in the air distribution within the curtain. The applicability of equivalent fluid models for bubble curtains is discussed, and it is shown that accounting for a gap in the bubble curtain, close to the manifold where the bubble curtain is not yet fully developed, results in better agreement between the modelled and the measured values of the insertion loss.

© 2025 Author(s). All article content, except where otherwise noted, is licensed under a Creative Commons Attribution (CC BY) license (https://creativecommons.org/licenses/by/4.0/). https://doi.org/10.1121/10.0035817

(Received 18 October 2024; revised 26 January 2025; accepted 27 January 2025; published online 20 February 2025)

[Editor: Nicholas P. Chotiros] Pages: 1336–1355

I. INTRODUCTION

The increasing demand for sustainable energy has led to a growing demand for offshore wind farms. Such installations are typically located in relatively shallow waters (<50 m), such that they can be bottom founded (Guo et al., 2022; Wang et al., 2010). For that reason, many coastal waters are being considered for the construction of wind farms, which can, for example, be seen in The European Marine Observation and Data Network (2023). The main method of securing the wind turbines to the bottom is by driving a monopile into the seabed using impact hammers (Merchant, 2019; Musial et al., 2019; Tsouvalas, 2020). The noise generated during this process significantly affects marine life (Dahl et al., 2015; Hastie et al., 2019; Popper et al., 2022). For this reason, other, less noisy methods of anchoring the wind turbines to the seabed are being developed (Igoe et al., 2013; Spagnoli and Weixler, 2013), but pile driving remains the dominant method to date. Bubble curtains have been proven to be effective in mitigating the negative effects of the noise fields generated during pile driving on marine life and are therefore widely used (Dähne

^{a)}Email: s.j.beelen@utwente.nl ^{b)}Email: d.j.krug@utwente.nl

1336

et al., 2017; Nehls et al., 2016). However, the operation of a bubble curtain adds significantly to the overall construction expenses. Typically, a separate vessel is required to install and operate the bubble curtain and the associated costs can easily exceed 100.000 euros per pile (Strietman et al., 2018). Efficient use of bubble curtains is therefore important to reduce the associated operating costs. However, reliable compliance with current (Juretzek et al., 2021) and future, possibly frequency dependent (Stöber and Thomsen, 2019; Tougaard and Dähne, 2017) regulations, is at least as high a priority and will remain a challenge.

There exists a multitude of acoustical models for predicting the sound emission due to pile driving, for which Tsouvalas (2020) presents a comprehensive overview. Although there are analytical relations for estimating the unmitigated emitted sound levels due to pile driving (von Pein et al., 2022), most predictions of the noise levels during pile driving rely on the finite element (FE) method (in Sec. IV, these FE methods will be discussed in more detail). However, validation of the applied models for marine pile driving, including a bubble curtain, is hindered by the lack of measurement data. Acquiring a complete dataset involves full scale measurements at sea and is therefore costly. Moreover, if measurements are carried out, the resulting data are often not publicly available (Lippert et al., 2016). The nature of the



²WaterProof Marine Consultancy & Services BV, IJsselmeerdijk 2, 8221RC, Lelystad, The Netherlands

³Acoustics and Underwater Warfare Division, TNO, The Hague, 2509JG, The Netherlands

⁴Institute of Aerodynamics, RWTH Aachen University, Wüllnerstrae 5a, 52062, Aachen, Germany

problem also makes it difficult to isolate the effect of the bubble curtain, as the results are also affected by sound transmission through the seabed (e.g., Peng *et al.*, 2021).

For the cases where experimental data are available, the results of sound mitigation by bubble curtains can vary drastically. Stein et al. (2015) measured the sound exposure levels in different directions surrounding a pile driving site with an active bubble curtain. They found the sound exposure level (SEL) to vary $\sim 10 \, \mathrm{dB}$, which they attribute to the shape of the bubble curtain and the irregular air input. This shows the significance of a proper installation of a bubble curtain for reliable compliance. Similarly, a proper implementation of the bubble curtain in acoustic models is important for a priori estimates of the sound levels. It is therefore appropriate to focus on the bubble curtain in order to optimise its implementation and thereby maximise its effectiveness in both real-world applications and models. Rustemeier et al. (2012) tested different air bubble curtain hoses for their sound mitigating properties in a 10 m-deep lake. They found a hose with a porous membrane, generating very small bubbles, to perform significantly better than all hoses with drilled holes of different sizes and spacings. Chmelnizkij et al. (2016) discuss the relevant mechanisms for bubble curtain effectiveness to be the reflection, scattering, and damping. Rustemeier et al. (2012) implemented a model, including the aforementioned effects, and compared it to his findings. To match the observed damping of the bubble curtain generated by the membrane, a bubble size distribution with much larger bubbles than observed, had to be assumed (bubble sizes increased by 1 decade). Rustemeier et al. (2012) possibly encountered the limitation of the so-called equivalent fluid model they implemented [the equivalent fluid modelling approach is more generally applied to predict the effective speed of sound in bubble curtains (Tsouvalas, 2020)]. Chmelnizkij et al. (2016) point out that most equivalent fluid models—including the ones accounting for damping due to bubble oscillations as the one in Rustemeier et al. (2012)—assume a large interbubble distance, such that bubble-bubble interaction can be neglected, which for typical void fractions observed in bubble curtains is not the case. The inter-bubble distance becomes more relevant, close to and at the resonance frequency, as the radiation cross section of the bubbles increase to significantly surpass their physical size. Feuillade (1996) derived a model that includes a term for the bubble-bubble interaction. However, he also indicates that around the resonance frequency, non-linearities, which are not captured by their model, become prominent.

Bubble curtains are effective acoustic barriers at low frequencies, due to the large mismatch in (specific) acoustic impedance between the water and the bubbly layer (e.g., Zhu *et al.*, 2023). Particularly at lower frequencies, which are most relevant in the case of pile driving with typical emission peaks between ≈ 100 and ≈ 500 Hz (Bailey *et al.*, 2010; Bellmann, 2014), reflection, resulting from this impedance mismatch, is the dominant factor in sound mitigation (Chmelnizkij *et al.*, 2016). A mismatch in acoustic

impedance is, in the case of bubble curtains, a consequence of the lower speed of sound in the bubbly mixture as compared to the speed of sound in the water column. The change in density can be neglected since the void fraction inside the bubble curtain is on the order of ~ 1 %. At the same time, it is well known that the dependence of the speed of sound of a bubbly mixture (c_m) on the void fraction (β) is non-linear (Wood and Lindsay, 1956), which can be simplified to $c_m \approx \sqrt{p_a/\rho_l \beta}$, with p_a representing the surrounding pressure and ρ_l representing the liquid density in the relevant void fraction range for bubble curtains of $0.01\% < \beta$ ≪ 100% (Wijngaarden, 1972). This non-linearity indicates that the mismatch in acoustic impedance is hardly dependent on the amount of air supplied to the bubble curtain, since the speed of sound remains relatively low anyway. A significantly higher speed of sound (closer to that of pure water) requires such a low air supply rate that for practical applications, it would likely not result in a developed bubble curtain at all. This is because distributing the air evenly over the manifold poses a problem at low air flow rates. In addition, due to the significantly lower mixing in weak plumes (Wang et al., 2019), the bubble curtain is much more prone to develop inhomogeneously. The independence of the acoustic impedance mismatch on the air flow rate also indicates that splitting up the total air flow rate between two manifolds would result in two acoustic barriers, with both close to the same impedance as a single bubble curtain. This approach seems from these considerations promising for increasing the effectiveness of the supplied air. However, quantifying the insertion loss (IL) of the acoustic barriers is not trivial. Carstensen and Foldy (1947) used bubble screens to test the effect of bubbles on sound propagation. However, the bubble sizes (\sim 0.5 mm) and void fractions ($\beta \ll 0.1 \%$) considered in this study differ significantly in magnitude from those typically employed in bubble curtains. Along with their experiments, a model was presented for the resulting sound attenuation. Commander and Prosperetti (1989) also model the reflection and transmission coefficient of an incoming sound wave based on the void fraction and bubble size distribution inside a homogeneous bubbly mixture. The model by Commander and Prosperetti (1989) is applicable for low void fractions (β < 0.1 %) and has not been tested for the application to bubble curtains. Furthermore, the effect of the void fraction distribution within the curtain on its sound mitigating properties is unknown. We will, therefore, investigate the possible effectiveness of generating a second bubble curtain while using the same combined air supply rate. Thereby, creating a "free" second bubble curtain, where the bubble curtains with half the total air flow rate have individually close to the same impedance difference as the bubble curtain supplied with the total air flow rate. Using two bubble curtains is already common practice (Bellmann, 2014). In order to comply with regulations, a double bubble curtain is one of the frequently used mitigation measures. Currently, the supplied air flow rate mainly depends on the local operating conditions (e.g., depth, current, distance to the source). The optimal use of the

compressed air from an acoustics point of view is not yet taken into account. In order to study this aspect, curtains with a relatively short distance between them, while maintaining the same total air supply rate, are considered in the present study.

The aim of this paper is to investigate whether we can increase the performance of a bubble curtain configuration while using the same amount of air. To do so, the quantities used to measure the performance are introduced in Sec. II. The experimental setup, used to test the performance of single and double bubble curtains, is introduced in Sec. III. In addition to measurements, we have also verified whether the intended effect can be captured by modelling. Details of these models are provided in Sec. IV. In Sec. V, the results of the measurements and the simulations are shown; in Sec. VI, the implications of the results are discussed; and finally, in Sec. VII, the main conclusions are presented.

II. APPROACH

In this paper, we will focus on the performance of configurations with one or two bubble curtains in relatively close proximity. A configuration performs better if it reduces more, or transmits less, sound. This can be represented by the frequency dependent IL, which we will present in decidecade bands. The IL can be based on either the sound pressure level (SPL), $L_{P,s}$, in the following, or the SEL, $L_{E,s}$, from now on. Generally, the SPL is used for "continuous" sound and the SEL is used for "impulse" sound. The IL is defined as

$$IL = L_{P,s,nc} - L_{P,s,c} \tag{1}$$

or

$$IL = L_{E,s,nc} - L_{E,s,c}, \tag{2}$$

where the subscripts "nc" and "c" stand for no curtain and curtain, respectively. The subscript "s" stands for sound; it is used to indicate the origin of the signal. The IL is thus the difference in SPL or SEL between having no bubble curtain employed and having an active bubble curtain. The SPL is defined as

$$L_{P,s} = 10 \log_{10} \left(\frac{\int_{f_1}^{f_2} P_s^2(f) df}{p_0^2} \right) dB,$$
 (3)

with $p_0 = 1 \,\mu\text{Pa}$ representing the reference sound pressure and P_s representing the sound pressure spectral density in the frequency domain (Fourier transform of the pressure in the time domain). f_1 and f_2 are the lower and upper bound of the considered frequency range. Finally, the SEL is defined as

$$L_{E,s} = 10 \log_{10} \left(\frac{\int_{t_0}^{t_1} p_s(t)^2 dt}{E_0} \right) dB,$$
 (4)

with $E_0 = 1 \,\mu\text{Pa}^2 s$, p_s , the time signal of the pressure. The time span that is used throughout this paper is defined as $\Delta t = t_1 - t_0 = 3 \, \text{s}$.

III. EXPERIMENTAL SETUP

The experiments reported on in this paper were carried out in the so-called concept basin (CB) of the Maritime Research Institute Netherlands (MARIN). The CB is a freshwater tank with a length of 220 m, a width of 4 m, and a depth of 3.6 m. Measurements were taken approximately in the middle of the tank, with the bubble curtains emanating from a pipe at the bottom of the tank.

The bubble curtain(s) were generated from a polyvinyl chloride (PVC) pipe with outer diameter, $d_{out} = 32 \,\mathrm{mm}$, and inner diameter, $d_{in} = 24.8 \,\mathrm{mm}$. The large wall thickness of the 3.6 mm pipe was one of the measures taken to be able to generate a continuous bubble curtain at low air flow rates since the larger resistance in the nozzle is favourable for an even air distribution along the length of the pipe. A bubble curtain assembly is shown in Fig. 1(a). It consists of the pipe with the holes (the manifold). That pipe is connected via two knee joints to the supply pipes. The first nozzle is drilled close to the knee joint to ensure that the bubble plume covers the entire width up to the basin walls. The distance from the wall to the first nozzle was less then the inter-nozzle spacing ($\Delta x_n = 100 \,\mathrm{mm}$). The supply pipes are designed to be screwed into the manifold pipe for ease of transport. The total width of the assembly is 3950 mm, to ensure the bubble curtain fits within the basin easily. The air is supplied from two directions into the manifold to reduce the effect of pressure drop over the length of the pipe. The two vertical supply pipes function as a pressure vessel, and reduce the effect of the inflow conditions on the generation of the bubble curtain as compared to directly attaching the air supply to the manifold. Both the pressure vessel effect and the reduced inflow effect contribute to a more continuous bubble curtain particularly at lower air flow rates. The height of the total assembly was approximately 4 m such that the connections of the supply pipes to the air supply were above the water.

In order to generate bubble curtains with both low and high flow rates, we decided to employ two manifolds per bubble curtain location. The first manifold, for the lower air flow rates, has a nozzle diameter of $d_n = 1$ mm and the second manifold has a nozzle diameter of $d_n = 2$ mm. These two were mounted together onto a weighted frame and then lowered to their position on the bottom of the tank. We mounted a light-emitting diode (LED) strip next to the manifold to visually inspect whether the generated bubble curtain was continuous [see Fig. 1(b)].

If possible, the air flow rate was controlled by a Bronkhorst F-203AC-FAC-50-V (Ruurlo, the Netherlands) (max flow rate 600 Lmin⁻¹) and otherwise monitored by an Omega FLR-1206 (Enschede, the Netherlands) (max flow rate 1400 Lmin⁻¹, max pressure 2.8 bar) and manually controlled using a ball valve. The air supply was either through the local pressurized air network at MARIN (up to 600 Lmin⁻¹) or by a

https://doi.org/10.1121/10.0035817

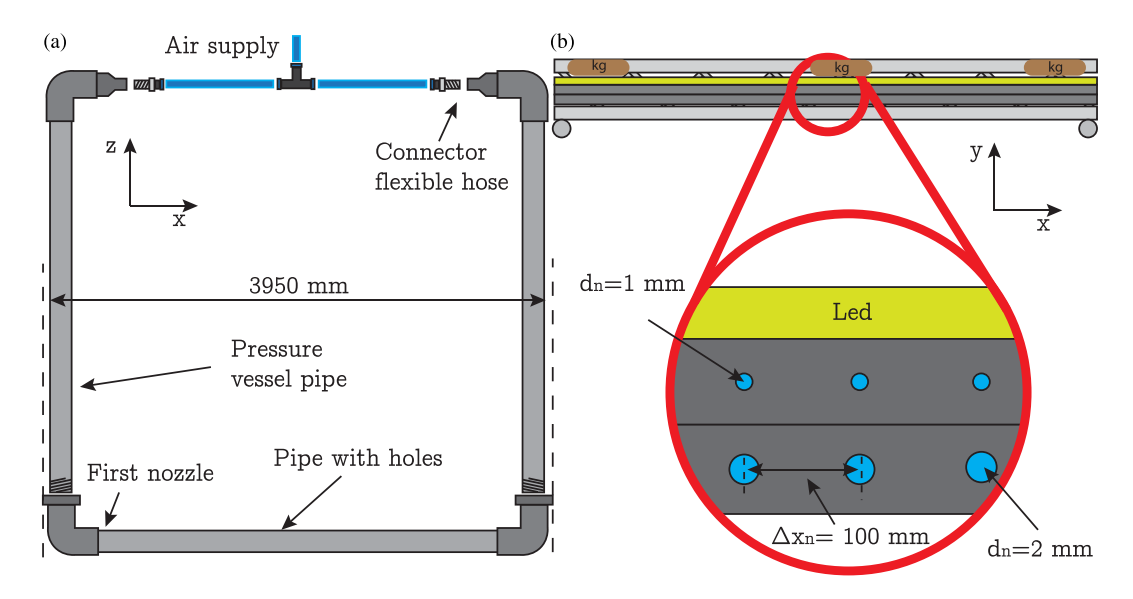


FIG. 1. (a) Bubble curtain assembly, (b) mounting of two bubble curtains on a weighted frame.

diesel air compressor (up to 900 Lmin⁻¹). For flow rates higher than 600 Lmin⁻¹, we generally used the manifolds with the 2 mm nozzles. To distribute the air to our bubble curtain assemblies, we used four ball valves, each of which could manually be opened to supply air to the desired bubble curtain. We only measured the total air flow. This means that if we use two bubble curtains at the same time, we do not know the exact distribution between the two. However, care was taken to ensure that only manifolds with the same nozzle diameters were used, that both ball valves were fully open, and that all the supply hoses were of the same length, so that we can assume that the air flow rate is approximately equally distributed to both bubble curtains.

In Fig. 2, the locations of the bubble curtains are shown. Bubble curtain 2 is only employed when we use two bubble curtains. The *x*-coordinate is running parallel to the manifold, the *y*-coordinate is perpendicular to the manifold, and the *z*-coordinate points upwards in the vertical direction. The *x*-coordinate originates in the center of the tank, the *y*-coordinate originates at the source location, and the *z*-coordinate originates at the bottom of the tank. The distance between both bubble curtains is $\Delta y_{bc} = 6$ mm.

Two different sound sources, a J11 hydro sounder/projector produced by the Underwater Sound Reference

Division (USRD, Bugg Spring in Okahumpka, FL) (see J11 hydrosounder, 2024) and a down-scaled airgun (TNO, Den Haag, the Netherlands) with a volume of 164 cm³ and an adjustable pressure (200-800 kPa), were used. The J11 hydrosounder was driven by a logarithmic sweep between 0.1–10 kHz in 10 s, as shown in Appendix A. The J11 also produced some (unintended) higher harmonics. The airgun was primarily used to evaluate the effectiveness of a bubble curtain at one time instance as opposed to the J11, which collects information over longer periods of time. Additionally, it was found to be useful in generating higher sound levels, especially at lower frequencies, in comparison to the J11 hydro sounder. During the measurements, we tuned the pressure of the pulse generated by the airgun such that the first receiver would not clip (overload). Both sound sources were located in the middle of the tank $(x_s = 0 \text{ m}, y_s = 0 \text{ m}, z_s = 1.8 \text{ m})$, the sources were never installed simultaneously.

The receivers we used were four Brüel & Kjaer 8106 hydrophones (Nærum, Denmark), the locations of the receivers are, in accordance with Fig. 2: $(x_{r,1}=0\,\mathrm{m},\ y_{r,1}=1.8\,\mathrm{m})$, $z_{r,1}=1.8\,\mathrm{m}$, $z_{r,2}=0\,\mathrm{m}$, $z_{r,2}=0\,\mathrm{m}$, $z_{r,2}=1.8\,\mathrm{m}$, $z_{r,3}=0\,\mathrm{m}$, $z_{r,3}=12.0\,\mathrm{m}$, $z_{r,3}=1.8\,\mathrm{m}$, and $z_{r,4}=0\,\mathrm{m}$, $z_{r,4}=18.0\,\mathrm{m}$, $z_{r,4}=1.8\,\mathrm{m}$.

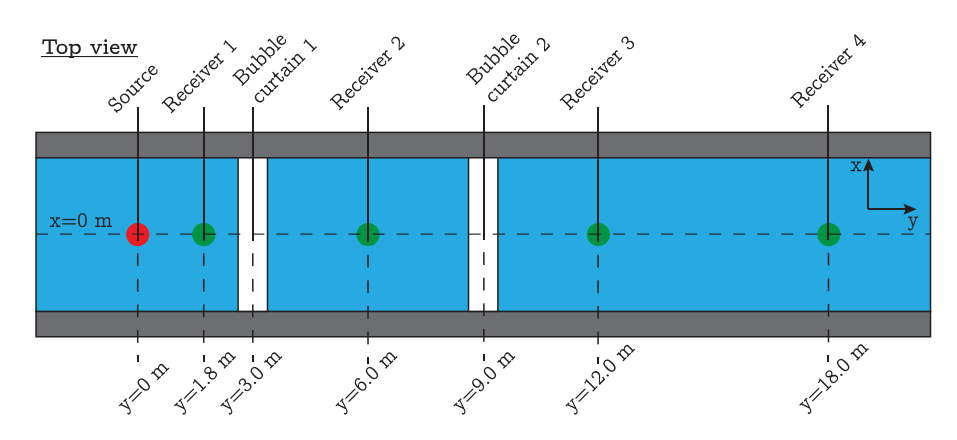


FIG. 2. Schematic overview of the setup in the concept basin.

The measurements with the J11 hydro sounder were recorded for 60 s; due to a minor delay in the signal, this resulted in five fully recorded sweeps. The mini airgun recordings took 5 s; however, only the first 3 s after the trigger were used in our analysis. We took recordings of the background noise levels for 30 s at three instances: (1) before the measurements, (2) between the measurements with the J11 hydro sounder and the mini airgun, and (3) after the measurements with the airgun. Finally, we also recorded the noise level of the bubble curtain(s) for 30 s directly before or after we carried out the measurements with the source, as to make sure we measured at exactly the same air flow rate. The hydrophones were calibrated using a piston-phone before and after the experiments.

IV. MODEL

To better understand the measurement results, we employ a model and compare the results with the measurement data. The model we employ is similar to most models used for sound emission predictions including bubble curtains found in the literature. Specifically, the use of the equivalent fluid model using, e.g., Commander Prosperetti (1989) (or related equivalent fluid models) is widely adopted in the literature. This approach involves characterizing the bubble curtain by its local speed of sound (e.g., Domenico, 1982). This approximation is valid in cases where the acoustic wavelengths are much larger than the typical bubble sizes (Wood and Lindsay, 1956). We use the same modelling approach as used for marine pile driving, albeit, without modelling the source excitation and without the necessity for a seabed model. Only the IL is considered (foregoing the need to know the source characteristics) and our experiments take place in a laboratory environment.

The modelled domain throughout this paper corresponds with Fig. 2 (top view) and is also shown in Fig. 9 (side view). The computational cost of the model is limited by using a so-called 2.5 D approach. In this approach, the full three-dimensional (3D) solution is approximated by summing over so-called "propagating modes." In this context, a propagating mode is defined as the combination of an assumed solution in x-direction that fits the boundary conditions on the side of the tank (acoustically hard) and the solution of an associated FE calculation for the y- and zdirection. In the FE calculation, the wave number, for the combined y- and z-direction, is the wave number in the medium reduced by the wave number in x-direction; this wave number will be referred to as the reduced wave number. Only modes with a real (reduced) wave number for the FE calculation are considered propagating modes. Modes for which the (reduced) wave number is complex decay exponentially in y-z-direction, thus leading to minor contributions to the total solution at larger ranges. The solutions of these propagation modes are cosines in the x-direction since the source and receiver are located in the center of the basin, thus requiring only symmetric modes to be included. Neglecting the evanescent modes reduces the computational

costs significantly. The number of included propagation modes in practice depends on the frequency of the sound. The FE method is known to converge to the true solution of the mathematical problem (i.e., the Helmholtz equation) and provides a good approximation for acoustic problems, as long as the mesh is generated carefully (see Appendix B). One of the benefits of the FE method for acoustic applications is that it is able to represent infinitely long wave guides efficiently using perfectly matched layers (PMLs), reducing the computational costs significantly. Moreover, implementation of the bubble curtain in the domain is relatively straightforward. The relevant details of the modelling approach will be provided in the following text.

A. Frequency content

The considered frequency range, in terms of the centers of the decidecade bands, is $31.5\,\mathrm{Hz} < f < 5000\,\mathrm{Hz}$. Within these decidecade bands, we chose to resolve five logarithmically distributed subfrequencies, and the energy/power spectral density in the associated subbands is assumed to be constant within these subbands. The higher frequencies are more computationally intensive since they require a relatively small mesh size due to the smaller wavelengths. It was therefore decided to limit our range to $5000\,\mathrm{Hz}$. This is acceptable since typical pile driving sound mainly contains low frequency components [$<2000\,\mathrm{Hz}$ (Bellmann, 2014)].

B. Acoustic representation of a bubble curtain

The bubble curtain is represented as an equivalent fluid by using an equivalent speed of sound c_m in the bubbly mixture. The speed of sound in the bubble mixture is a complex number where the imaginary part represents the damping component. To determine c_m , we employ the well-known model of Commander and Prosperetti (1989), in which the bubble response is linearized. According to this model, the sound speed depends on the frequency, f, the gas fraction, ϵ_g , and the probability density of the bubble size distribution, f_{num} . The latter two can be combined into the bubble concentration (number of bubbles of a certain size per unit volume)

$$C(a,x,y,z) = \frac{\epsilon_g(x,y,z)}{4/3\pi \int_0^\infty a^3 f_{\text{num}}(a,x,y,z) da} f_{\text{num}}(a,x,y,z),$$
(5)

where a is the bubble radius undisturbed by the sound pressure. The local void fraction in the bubble plume can be modelled using a planar plume integral model. To that end, we use the model derived and validated in our previous work (Beelen and Krug, 2024), which is based on the integral equations starting from individual round plumes giving us the local void fraction $\epsilon_{\rm g}(x,y,z)$. The model also predicts the local bubble size distribution, albeit only as a function of the vertical position above the nozzle $[f_{\rm num}(a,z)]$. This is consistent with the observed limited variation in the bubble

size distribution in the spanwise (y) direction (e.g., Beelen *et al.*, 2023). The model thus provides a full bubble concentration profile throughout the bubble curtain. The local speed of sound of the mixture $c_m(f, C)$ is given by

$$\frac{c^2}{c_m^2} = 1 + 4\pi c^2 \int_0^\infty \frac{aC(a)}{\omega_0^2 - \omega^2 + 2ib\omega} da,$$
 (6)

where $\omega = 2\pi f$ is the radial frequency, $c = 1481 \,\mathrm{m/s}$ is the speed of sound in water, and i is the imaginary unit. The eigenfrequency, ω_0 , and damping coefficient, b, of the bubbles in the mixture are defined as

$$\omega_0^2 = \frac{p_0}{\rho a^2} \left(\text{Re}\Phi - \frac{2\sigma}{ap_0} \right) \tag{7}$$

and

$$b = \frac{2\mu}{\rho a^2} + \frac{p_0}{2\rho a^2 \omega} \operatorname{Im}\Phi + \frac{\omega^2 a}{2c}.$$
 (8)

 $p_0=p_\infty+2\sigma/a$ is the undisturbed pressure in the bubble, $p\infty$ the equilibrium pressure in the surrounding liquid, and $\sigma=72.8\,\mathrm{mN/m}$ the surface tension of the bubble. $\rho=1000\,\mathrm{kg/m^3}$ and $\mu=1\,\mathrm{mPas}$ are the density and viscosity of the surrounding water. The complex valued function Φ describes the heat transport inside the bubble,

$$\Phi = \frac{3\gamma}{1 - 3i(\gamma - 1)\xi\left(\sqrt{i/\xi}\coth\sqrt{i/\xi} - 1\right)},$$
(9)

and depends on the specific heat ratio of air, $\gamma=1.4$, and $\xi=D/\omega a$ with $D=18.46\cdot 10^{-6}~\text{m}^2/\text{s}$ representing the thermal diffusivity of air. The damping constant [Eq. (8)] comprises three terms representing, from left to right, the viscous damping, damping due to heat dissipation, and damping due to acoustic radiation.

For effective implementation, it is important to note that the integral in Eq. (6) does not need to be evaluated at every horizontal location. This is because the bubble size distribution is assumed to only vary with the vertical distance from the nozzle in the model. Therefore, the following representation, where the void fraction is outside of the integral, significantly reduces the computational cost of calculating the equivalent speed of sound at many different locations throughout the curtain, which is the required input to the FE model

$$\frac{c^2}{c_m^2} = 1 + \epsilon_g 4\pi c^2 \int_0^\infty \frac{a f_{\text{num}} / \left(4/3\pi \int_0^\infty a^3 f_{\text{num}} da\right)}{\omega_0^2 - \omega^2 + 2ib\omega} da. \quad (10)$$

For a given bubble size distribution and void fraction distribution, we retrieve a distribution of the speed of sound in the mixture $[c_m(x, y, z)]$. As previously discussed, we utilise a two-dimensional (2D) FE model to compute the sound propagation. To reduce the 3D situation to a 2D representation, we first calculate the average void fraction in the

x-direction and then compute the corresponding speed of sound. This choice is substantiated in Appendix C, where the effect of structures (or "holes") in the void fraction distribution of real bubble curtains is discussed in relation to this choice. We further focus in on the difficulties associated with reducing a 3D situation to the 2D FE domain.

C. Implementation and results

The FE model is implemented in COMSOL Multiphysics 6.0 (Göttingen, Germany). This commercially available software allows for easy FE implementation of acoustic problems. For the sake of brevity, the detailed implementation is discussed in Appendix B. The numerical domain (see Fig. 9 in Appendix B) covers the full experimental configuration in the *y-z* plane. The speed of sound within the bubble curtain is calculated according to Eq. (10). The performance of the bubble curtain will be presented in terms of the IL as discussed in Sec. II. The IL is calculated based on the SPL [Eq. (1)] or the SEL [Eq. (2)].

D. The effect of "holes" in the bubble screen

Close to the manifold, the bubble plume is not yet continuous leaving "holes" in the x-z-plane of the bubble curtain. These holes in between the individual nozzles do not contain bubbles and possibly reduce the effectiveness of the bubble curtain. We capture the fraction of "open," i.e., largely void of bubbles, surface area in the bubble curtain in terms of a transparency factor. As shown in Appendix C, there is no direct way of incorporating transparency directly through the effective speed of sound in a 2D FE simulation. To assess the impact of openings in the curtain, at least approximately, we introduce a gap filled with water containing no bubbles at the bottom of the modelled bubble curtain. Based on the approximate distance at which individual plumes merge (Beelen and Krug, 2024), this gap extends $2\Delta x_n = 200 \,\mathrm{mm}$ upwards from the manifold and we set $c_m = 1481 \,\mathrm{ms^{-1}}$ in this region. This approach is in line with scenario 3 of Peng et al. (2021), who also represent the zone of individual plumes as a leakage region, which is characterized by the acoustic properties of water.

V. RESULTS

In this section, we will present the results of the measurements focusing on the IL and compare to model predictions where relevant. As given by Eqs. (1) and (2), the IL is the difference between the sound levels with and without a bubble curtain. In practice, however, the measured levels may be significantly influenced by the background noise levels. In order to suppress the effect of the background noise on the measured spectrum, we subtract it from our measured signal, $P_s^2 = P_{s+n}^2 - P_n^2$, where P_{s+n} is the measured pressure spectrum resulting from the sound of the source and the background noise and P_n is the background noise pressure spectrum. P_s is the Fourier transformed sound pressure (Pas) due to the source and can be used to determine the IL [Eq. (1)]. The IL based on the SEL [Eq. (2)] is corrected for the background noise levels similarly to the

SPL and the term p_s^2 in the integral is replaced by $p_s^2 = p_{s+n}^2 - p_n^2$ to correct the SEL for noise. These approximations are accurate when the sound level and the background noise level are uncorrelated. Furthermore, the correction is only meaningful if the sound level of the signal of interest is higher than the sound level of the noise.

The background noise levels (shown in Appendix D) are measured when the sound source and bubble curtains are not active. The maximum recorded background noise (Bg, max in the following figures) across measurements at different times is used as the depicted background noise level in the following text. The noise generated by the bubble curtains is also considered background noise. As shown in Appendix E, the noise level is flow rate dependent. In particular, for the 1 mm nozzle manifold, we observe a strong dependence on the air flow rate, whereas the noise is only weakly dependent on the air flow rate when using the 2 mm nozzles. If the transmitted sound level from the source at a receiver approaches the noise level, the contribution of the source becomes indistinguishable, and the correction for noise proposed above becomes invalid. The source is considered indistinguishable if the total received sound level is less than the 3 dB higher than the background noise level $(L_{P,s+n} < L_{P,n} + 3 \text{ dB})$. When this condition is met, we set $L_{P,s} = L_{P,n}$ (similar for SEL) to clearly indicate the signalto-noise limitation. Regions where the sound of the source is no longer distinguishable from the noise will also be indicated by a gray area in the following figures.

The sound generated by the sources without the bubble curtain active is explicitly used in the definition of the IL $[L_{P,s,nc}]$ and $L_{E,s,nc}$ in Eqs. (1) and (2), respectively] and is shown in Appendix F for the fourth receiver. Between different sweeps or different shots of the airgun, the produced signal changes slightly. Therefore, we will use the average

sound levels of five sweeps or six shots of the airgun in (most of) the following analysis to determine the IL. Variations in the generated signal are particularly relevant for the airgun as we will present in Sec. VB. The 3 s time interval for the SEL is chosen such that it captures the full event of approximately 1 s with sufficient resolution in the frequency domain, while maintaining a limited influence of noise. At lower frequencies (<250 Hz), the airgun generates significantly more sound than the hydrosounder and also at higher frequencies, the level remains somewhat higher (see Appendix F).

In the following, we will first show an example of the sound pressure levels used to determine the IL so that we can show the general trend for all measurements and then move to the measured and modelled IL.

A. Sound pressure levels throughout the measurement domain

In Fig. 3, we show the sound pressure levels at all four receivers without, with one, and with two bubble curtains for an air flow rate of 96 Lmin⁻¹, measured with and without the hydrosounder.

The IL at every receiver is given by subtracting the sound level without a bubble curtain (green and black dashed lines) from the sound level with a bubble curtain (solid blue line or solid blue line with black dots for one and two curtains, respectively). When operating a bubble curtain, the overall SPL at the first receiver [Fig. 3(a)] increases for frequencies exceeding 250 Hz due to reflection of the sound at the bubble curtain. The second receiver [Fig. 3(b)] is placed behind the first bubble curtain, which reduces the SPL when it is active. When the second bubble curtain is operated additionally, the SPL between both curtains is seen

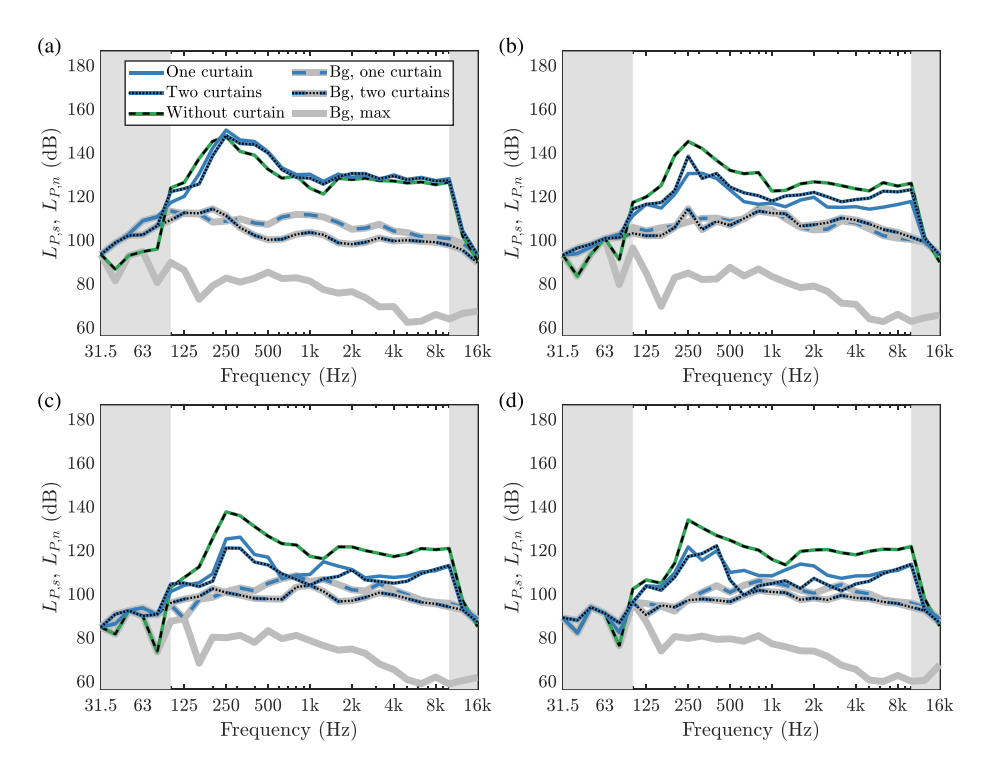


FIG. 3. Sound pressure levels for one or two bubble curtains with a total air flow rate of 96 Lmin⁻¹, without a bubble curtain and noise levels at (a) receiver 1, (b) receiver 2, (c) receiver 3, (d) receiver 4.

to increase. The increase is likely due to the reflection of sound at the second curtain and marginally due to reduced effectiveness of the first curtain resulting from the reduced air flow rate. The third receiver [Fig. 3(c)] is positioned behind both curtains and records lower sound levels overall, as expected, when using two bubble curtains. At the fourth receiver [Fig. 3(d)], we mostly observe a lower SPL when operating two bubble curtains, similar to the third receiver. The trends discussed here for an air flow rate of 96 Lmin⁻¹ are similarly observed for all air flow rates. However, the bubble curtain noise becomes more problematic for our measurements when the air flow rate is increased and a louder source would be required to ensure a good signal-tonoise ratio for these cases. This can already be seen in Fig. 3(d), where the SPL gets very close to the bubble curtain noise level around 630 Hz. For higher air flow rates, the region of the plot where the signal of interest is not above the noise floor extends to more frequencies. So far, in this section, we have shown a few examples of the sound pressure levels, which can be used to calculate the IL. In the next part of this section, we will present the measured and modelled IL for different air flow rates and source types.

B. IL based on hydrosounder measurements

We can calculate the IL from the sound levels plotted in Fig. 3. The general trend in Fig. 3 is seen for all air flow rates: The IL at the first receiver is negative due to reflection of the sound at the bubble curtain. The IL at the second receiver is positive, i.e., the sound level is reduced, and the value is higher for one bubble curtain than for two. At the third and fourth receivers, the IL is also positive and the two bubble curtain setup outperforms the one bubble curtain setup.

In Figs. 4(a) and 4(b), we show the IL for receiver 4 and 3, respectively. We will focus mainly on the IL measured at the fourth receiver since it is farthest away from the bubble curtain and we assume the performance of a bubble curtain further away from the source to be more relevant to the real-life application of bubble curtains. However, since the IL depends on the receiver location, the IL at both receiver locations 3 and 4 is shown once.

Particularly in the range of 0.5–4 kHz, the IL increases significantly. In the relevant frequency range of 0.1–3 kHz, the IL of both the one and two bubble curtain setup varies between 3 and 15 dB and 3 and 20 dB, respectively. Further, we see a dip in the IL around 1250 Hz, the precise origin of which is unknown. The source level around 1250 Hz also contains a dip (see Fig. 3), possibly indicating that the source is interacting with a resonance of the basin geometry.

For the low air flow (96 L/min) rate, the IL derived from the measurements is hardly influenced by the noise generated by the bubble curtains. For frequencies where the noise influences the IL derived from the measurements, we display the IL as a dashed line. In Fig. 4(c), the IL for an air flow rate of 396 Lmin⁻¹ is shown and as indicated by the dashed lines, it is for most frequencies limited by the noise

generated by the bubble curtain(s). Once the IL is limited by the bubble curtain noise, it should be interpreted as a lower bound for the actual IL. A louder source would be required to accurately determine the true IL in these cases. Still, the measured values are meaningful in the sense of a minimum IL of the bubble curtain and is therefore shown.

To illustrate the effectiveness of splitting up the air flow rate, the IL of a single bubble curtain configuration is subtracted from the IL of the two bubble curtain configuration, $IL_2 - IL_1$. This is shown for both 96 and 396 Lmin⁻¹ in Fig. 4(d). For air flow rates higher than 396 Lmin⁻¹ (not shown), both the one and two curtain IL derived from the measurements are limited by the noise floor such that the difference between the two is no longer meaningful and therefore not included. In Fig. 4(d), the dashed line indicates that the noise floor influenced the results. The difference in IL for the two air flow rates shown is mostly positive, meaning splitting up the air into two distinct bubble curtains increases the effectiveness of the compressed air used. For the frequencies 630 and 1600 Hz, the increase in IL even exceeds 11 dB at an air flow rate of 96 Lmin⁻¹. For 396 Lmin⁻¹, the difference is less distinct since the IL of the two bubble curtain setup was limited by the noise floor; nevertheless, significant IL increases exceeding 6 dB are observed. For both flow rates, the two bubble curtain setup performs worse than the one bubble curtain setup between 250-400 Hz. We will comment on these observations in Sec. VI.

C. Results for the IL based on the model

Also, included in Figs. 4(a)–4(c) is a comparison between the measured and the modelled IL. This is most informative for the lowest air flow rate [Figs. 4(a) and 4(b)], since the noise generated by the bubble curtain does not affect the measurement of the IL in this case. For frequencies between 500 and 3150 Hz, the IL of a single bubble curtain is overpredicted significantly and the dip in the measured IL centered around 1250 Hz is not seen in the model. The two bubble curtain setup also outperforms the single bubble curtain setup for frequencies exceeding 250 Hz in line with the measured IL. Comparing Figs. 4(a) and 4(b), we notice that the IL also depends on the receiver location in the model. In general, the qualitative trend for the variations in the sound pressure levels at the different receivers (see Fig. 3) is captured by the model.

From Figs. 4(a) and 4(c), it becomes clear that the modelled IL depends on the air flow rate and changes in this quantity not only affect the magnitude but also the frequency dependence of the modelled IL. A similar dependence was not observed in our measurements. To better understand the discrepancy between the measurements and the model, we turn to the version of the model for which we included a gap in the curtain close to the manifold (see Sec. IV D). The corresponding model result at an air flow rate of 96 Lmin⁻¹ at receiver 4 is compared to the results shown in Fig. 4(b) for the one bubble curtain configuration in Fig. 5.

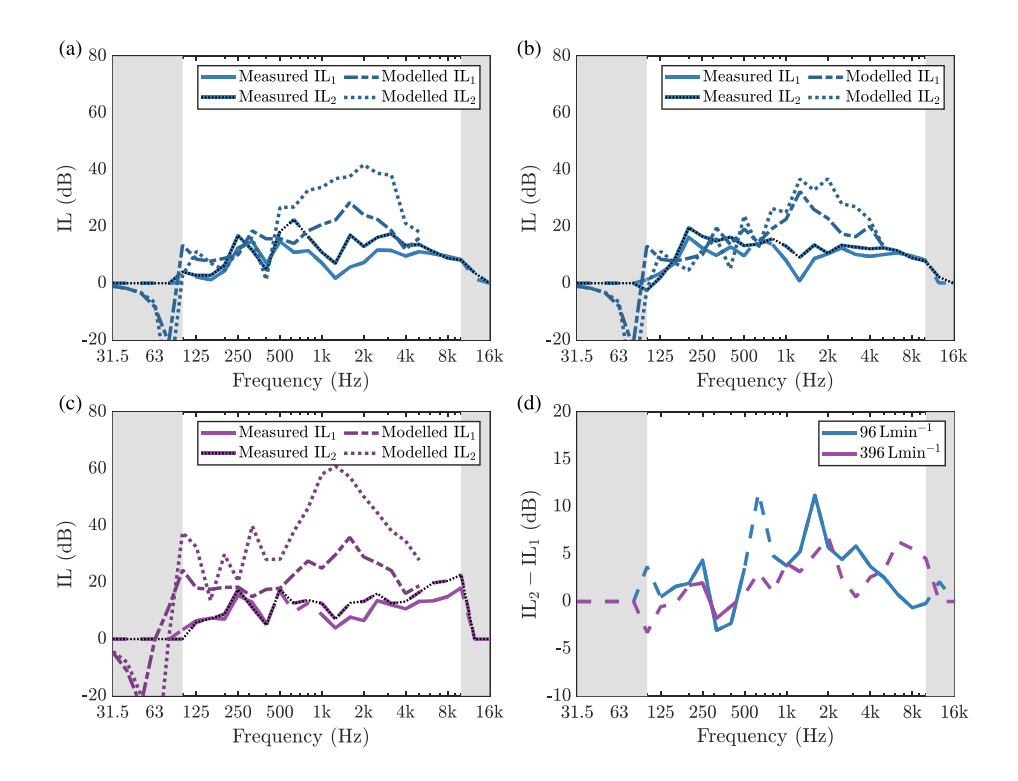


FIG. 4. The measured and modelled IL for different configurations with an air flow rate of 96 Lmin⁻¹ at (a) receiver 4 and (b) receiver 3. (c) For an air flow rate of 396 Lmin⁻¹ at receiver 4. (d) The measured difference in IL at receiver 4 for one and two bubble curtains.

It can be seen that including the gap results in a better agreement of the modelled IL with the measured data. Up until \sim 600 Hz, the influence of the gap is minimal in the model; however, for larger frequencies, a significant drop in the IL is observed if the gap is included. The frequency of \approx 600 Hz, at which the gap becomes important, does not correspond directly to the length scale of the $(1481/0.2 \approx 7500 \,\mathrm{Hz})$, but this cutoff is found to decrease with increasing gap height (not shown). Wang et al. (2023) looked into the effect of a gap more closely. When including the gap, the modelled IL for frequencies exceeding 600 Hz becomes largely independent of the air flow rate. Including the gap in the model improves the resulting prediction for

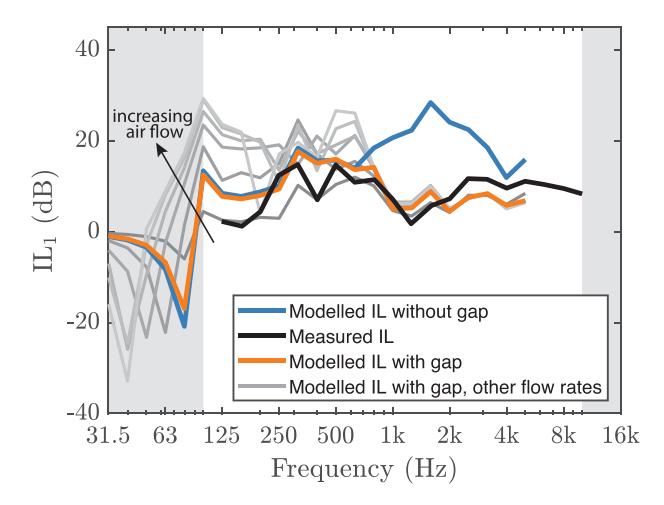


FIG. 5. IL of the one bubble curtain configuration; we compare the model with and without a gap in the bubble curtain to the measured IL at an air flow rate of 96 Lmin⁻¹. The gray lines are the results for different air flow rates.

the measured IL. Even if the present way of accounting for this effect is rather crude, these results highlight the importance of accounting for openings in the bubble curtain in the modelling.

In the following, we will show model results in order to compare the one and two bubble curtain setups from a modelling point of view. Both configurations are tested with and without the gap. The modelled IL without the gap for a single bubble curtain is shown for all flow rates in Fig. 6(a). In Fig. 6(b), the IL is shown for two bubble curtains employed; in Fig. 6(c), the difference in IL is shown.

The modelled results show, similar to the measurements, that the two bubble curtain setup increases the IL significantly. Contrary to the measurements, the IL does depend on the air flow rate [as also seen in Figs. 4(a) and 4(c)]. For frequencies exceeding \sim 250 Hz, the model shows an improved IL when using two bubble curtains. The large dip below 125 Hz in the difference in IL is mainly a consequence of the shifting of the dips between using one and two bubble curtains.

Figures 6(d)–6(f) show the results for the model with the gap similar to Figs. 6(a)-6(c). For both the one [Fig. 6(d)] and two [Fig. 6(e)] bubble curtain configurations, the IL becomes flow rate independent for the higher frequencies. However, when employing two bubble curtains, the IL becomes negative for higher frequencies. Such behaviour may be expected at lower frequencies due to a possible reduction of the impedance mismatch between the source and the medium. However, the origin of this phenomenon at higher frequencies remains unclear. Results for the model, including the gap, suggest that for higher frequencies, inserting two bubble curtains might actually be worse than no bubble curtains since the IL becomes negative; but this is

https://doi.org/10.1121/10.0035817

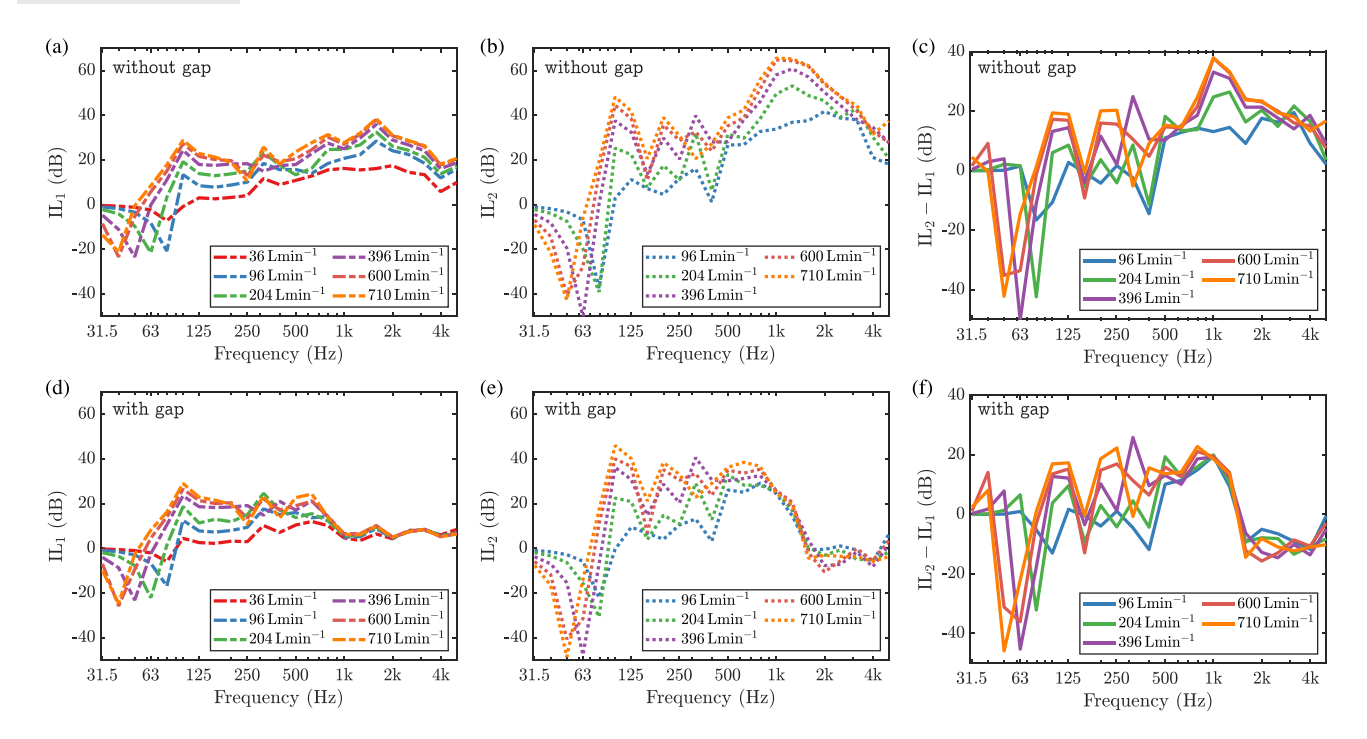


FIG. 6. The modelled IL for (a) one bubble curtain without gap, (b) two bubble curtains without gap, (c) difference in IL between different configurations without gap, (d) one bubble curtain with gap, (e) two bubble curtains with gap, (f) difference in IL between different configurations with gap.

not seen in our experiments [Fig. 4(d)]. For the lower frequencies, the effectiveness of splitting up the air flow rate is largely retained even when the gap is included.

The sharp negative peaks around $\sim 80 \,\mathrm{Hz}$ in Figs. 6(a), 6(b), 6(d), and 6(e) appear in the IL predicted by the models with or without gap. We could not confirm the presence of such a peak experimentally, since the source does not generate sufficient sound pressure at these low frequencies.

D. Airgun measurements

So far, we have focused on the results measured by the hydrosounder since the source signal is more repeatable, resulting in more reliable measurements (see Appendix F). However, an advantage of the airgun is that it generates more sound, particularly at lower frequencies, and the corresponding results are therefore discussed in the following text.

In Figs. 7(a) and 7(b), we show the IL at the fourth receiver for different air flow rates for one and two bubble curtains, respectively. For frequencies exceeding $\sim 500\,\mathrm{Hz}$, for increasingly more flow rates, the IL derived from the measurements is still determined by the noise floor, even when using the slightly louder airgun. Nevertheless, the data show that, where measurable, the IL is indeed hardly flow rate dependent. A deviation from the flow rate independent IL can be seen for frequencies exceeding $2\,\mathrm{kHz}$ by comparing 36 and $96\,\mathrm{Lmin}^{-1}$ in Fig. 7(a). This could indicate the importance of damping at higher frequencies, but this seems unlikely as it is not consistent with our previous observations and is not supported by the results from the model with and without a gap. An alternative, more likely explanation is that the bubble curtain was not fully developed at this low

air flow rate, underlining the relevance of openings in the curtain discussed in Sec. V C. Comparing Figs. 7(a) and 7(b) paints a similar picture as to the measurements with the hydrosounder in that the overall IL increases when splitting up the air flow over two manifolds.

In Fig. 7(c), the IL is plotted for individual shots of the airgun alongside the average IL with the airgun and the hydrosounder for the lowest air flow rate of a single bubble curtain (36 Lmin⁻¹). Quantifying these variations is important since they cannot be predicted by models using average descriptions of the bubble curtain. There are two main possible sources of variation in the presented IL: The (non) repeatability of the source and the variations in the bubble curtain composition. It is known that the source level spectrum becomes less repeatable for subsequent shots for frequencies exceeding 630 Hz for this particular airgun (see Appendix F). To distinguish the two sources of variation, we show two properties. The spread in the IL will be defined as maxIL-min IL for the individual airgun shots and is shown in Fig. 7(d), which we call the IL based result. The variations can be as much as 7 dB. To estimate the contribution of the variation in the sound source to the spread in the IL, the spread in the difference between the SEL at receiver 1 and 4 is plotted. Since both of these levels are measured using the same source signal, the spread is therefore more likely to be mainly due to time dependent properties of the bubble curtain(s) (in Appendix G, we discuss the relevance of this property in more detail). Even though the variations determined in this way are generally lower, they can still exceed 4 dB, suggesting changes in the composition of the curtain play a significant role in the observed spread in IL.

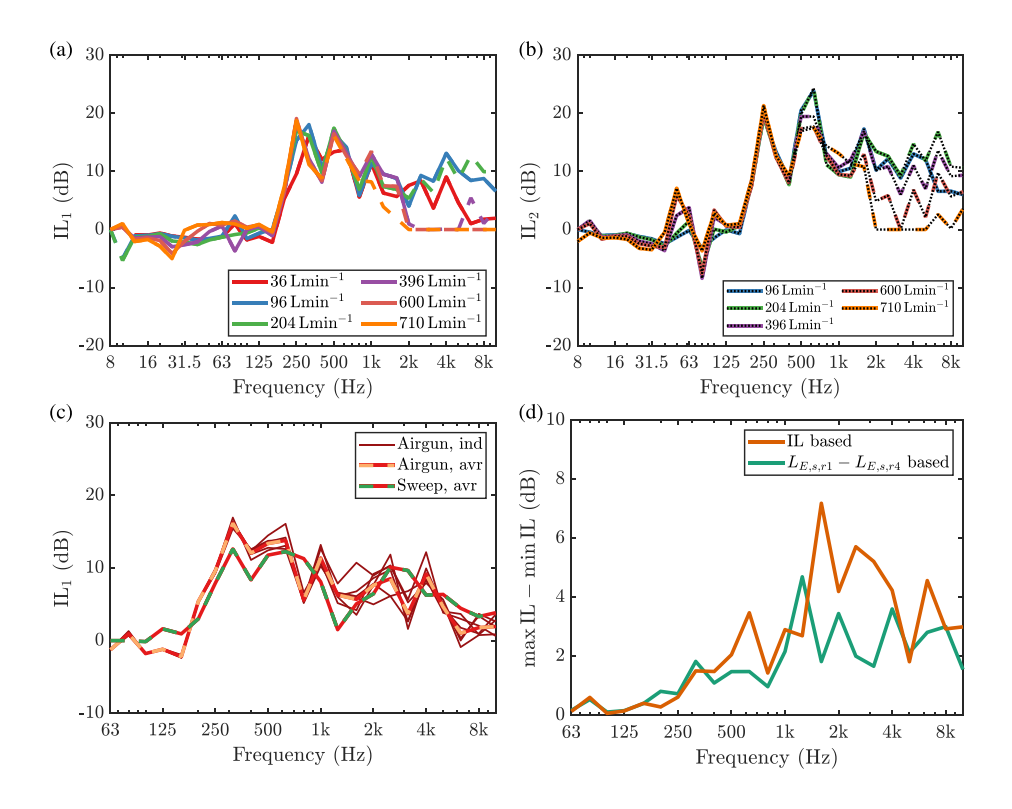


FIG. 7. The measured IL by using the airgun for different air flow rates: (a) for a single bubble curtain, (b) for two bubble curtains, (c) the IL of individual airgun shots and average IL both for the airgun and hydrosounder having a single bubble curtain employed at the lowest air flow rate $36 \, \mathrm{Lmin}^{-1}$, (d) the maximum variation in IL based on the six individual airgun shots.

VI. DISCUSSION

In this section, we will discuss the results with regard to our objective of investigating the effect of a two bubble curtain configuration. However, we cannot interpret these results without considering the limitations resulting from our experimental setup.

A. Remarks on the experimental setup

Some of the advantages of measuring inside a basin are the repeatability, the known geometry, and the low noise floor. In addition, hydrodynamic measurements can be conducted alongside acoustic measurements in a fresh water environment for which our hydrodynamic model (Beelen and Krug, 2024) was validated previously. However, the measured acoustic

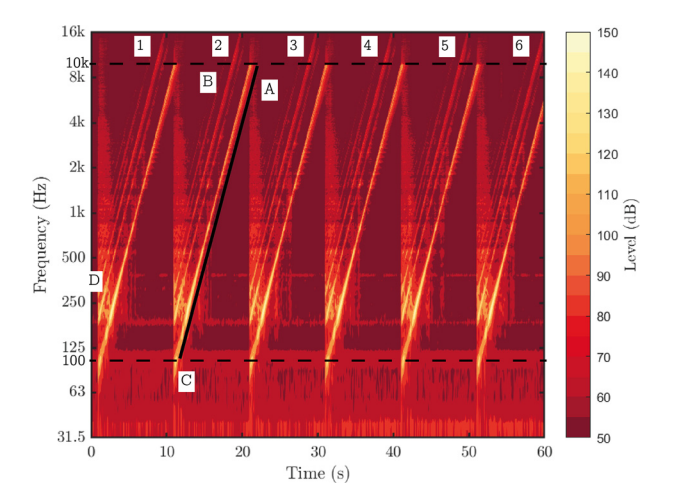


FIG. 8. Decidecade band spectrogram of the sound pressure sweeps from the J11 hydrosounder, recorded by receiver 2 without a bubble curtain active.

performance of bubble curtains might differ from those measured at full scale. The basin does not directly compare to the use-case of interest, being impact pile driving in ocean waveguides.

To be more precise, the bubble curtain is placed inside a basin and its performance cannot be seen independent of this environment. Placing an omni-directional sound source, such as the ones used here (for the frequency range of interest), in an enclosed basin leads to an interference pattern due to interactions of the sound field directly radiated by the source and its reflections on the side walls and on the water surface. As a result, the amplitude of the sound field strongly depends on the measurement location within the interference pattern. This becomes problematic when interpreting the IL since the presence of a bubble curtain alters the interference pattern. A location at which constructive interference happens at a specific frequency without the curtain may exhibit destructive interference when the curtain is present, and vice versa. The IL, therefore, does not only represent the change due to inserting a curtain for the direct path, but is also influenced by the change in contributions of paths resulting from interaction with the basin walls and the water surface. The influence of secondary paths can be suppressed by adding an array of hydrophones behind the curtain/curtains in future measurements instead of a single hydrophone. Such a setup could potentially give insight in the relative contribution of the direct path vs other paths.

Having observed the different IL curves based on measurement and model data, we notice that they are very spiky, which could partially be caused by the interference between different sound paths. We believe that despite the influence of the basin environment, the trends in the IL as measured in the basin are qualitatively relevant for comparative analysis

https://doi.org/10.1121/10.0035817

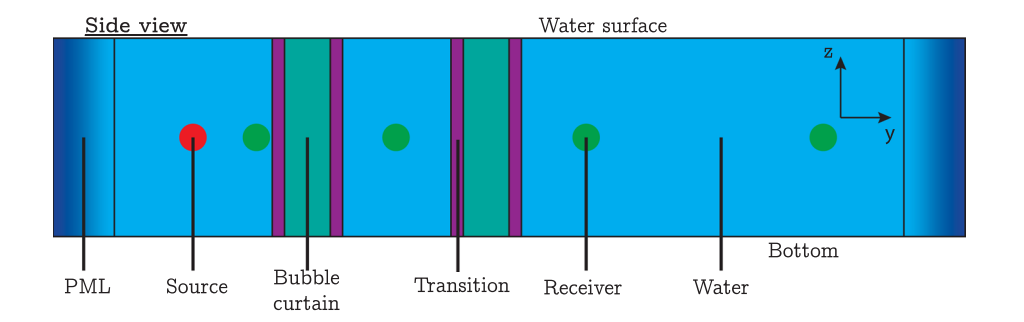


FIG. 9. Illustration of the modelled domain and the locations of the source and receivers

between different cases and real-life bubble curtain applications. For instance, while the difference in IL curves for one and two bubble curtains might be very different for specific frequencies due to changes in interference patterns, the overall observed trend is that the IL is higher for a two bubble curtain setup.

In addition to the effect of the influence of the environment on the IL, it was also observed that for most air flow rates, both sources used during the measurement are incapable of generating a signal at the other side of the curtain that exceeds the noise generated by the bubble curtains. This implies that an accurate assessment of the IL over the complete frequency range cannot be made for many of the investigated cases.

B. Effect of one or two bubble curtains

With the experiments, we set out to test the effect of different bubble curtain configurations on the IL. As can be seen in Fig. 4(d), the effect of splitting the total air flow rate over two distinct bubble curtains is considerable. Splitting up the air flow into two separate bubble curtains generally increases the performance of the supplied air within the measurable range. The effect of the split, however, does not manifest itself as a constant increase in IL that is observed for all frequencies. Moreover, there are decidecade bands, for which the increase is high with neighboring bands for which the increase is almost zero or for which a decrease is observed. A conspicuous deviation to the increased performance of the bubble curtain when the supplied air flow rate is increased occurs around 250-400 Hz. This corresponds roughly to $c/\Delta_{bc} \approx 250 \, \text{Hz}$, which seems to be an eigenfrequency of the system with inter-curtain distance, Δ_{bc} . The main reason as to why this split up of the total air flow rate is effective is due to the non-linear relation between the speed of sound and the local void fraction, as mentioned in the Introduction. For a typical void fraction along the centerline of the curtain of \sim 1%, the local speed of sound, according to Wood and Lindsay (1956), is $c_m \approx 120 \, \mathrm{ms^{-1}}$. Halving the void fraction to 0.5% results in a speed of sound of $c_m \approx 170\,\mathrm{ms}^{-1}$. Both of these remain low, as compared to the speed of sound in water of $c = 1481 \,\mathrm{ms}^{-1}$, and therefore maintain a large impedance mismatch. Primarily, the positive effect of adding a second bubble curtain can therefore be explained by the maintained impedance mismatch for each bubble curtain even as the air flow rate per curtain is reduced. This effect is mainly important for the lower frequencies (<1000 Hz), for which reflection is the dominant mechanism for sound reduction. The independence of the IL from the air flow rate, as seen in Figs. 7(a) and 7(b), is another indication of the probable importance of this mechanism. The observed flow rate independence of the IL, however, must be interpreted with caution, since the experimental setup may influence this conclusion. Nevertheless, Rustemeier et al. (2012), e.g., reach similar conclusions and report only a small dependence of the IL on the air flow rate, compared to the large dependence on the configuration. For increasing frequency, approaching and exceeding the eigenfrequencies of the present bubbles, the split up of the air flow rate is expected to be less effective as damping becomes more relevant compared to reflection. For very low frequencies ($f \ll c/\Delta_{bc}$), the two bubble curtains might act as one. The latter point, as well as the observed lower performance around the eigenfrequency of the system, demonstrate that the distance between the two manifolds influences the performance of the system.

The model predicts an increased effectiveness of splitting up the air flow rate into two bubble curtains just as the measurements show. The magnitude of the improvement, and the absolute values of the IL are, however, overpredicted by the model. The very significant increase in IL when using two manifolds is interesting for real-life applications of bubble curtains. The results show that compressed air can be used more effectively when it is split up in two distinct bubble curtains. Splitting the air over even more manifolds, while keeping the inter-bubble curtain distance the same, could prove to be an even more effective use of the compressed air.

C. Model vs reality

In Fig. 7(c), we showed the large variation in the IL for individual shots with the airgun. This spread originates from both the variation in the source sound levels and the variability of the effectiveness of the bubble curtain, as shown in Fig. 7(d). We used a time interval of 5 s between different instances of the airgun, such that effectively, all the air inside the bubble curtain has been replaced (3.6 m deep with a rising velocity of $\sim 1 \, \mathrm{ms}^{-1}$). Each sound pulse thus "sees" a new and different bubble curtain. Some of the effects that change the bubble curtain in time are the wandering, the cloud-like structures with locally different bubble densities,

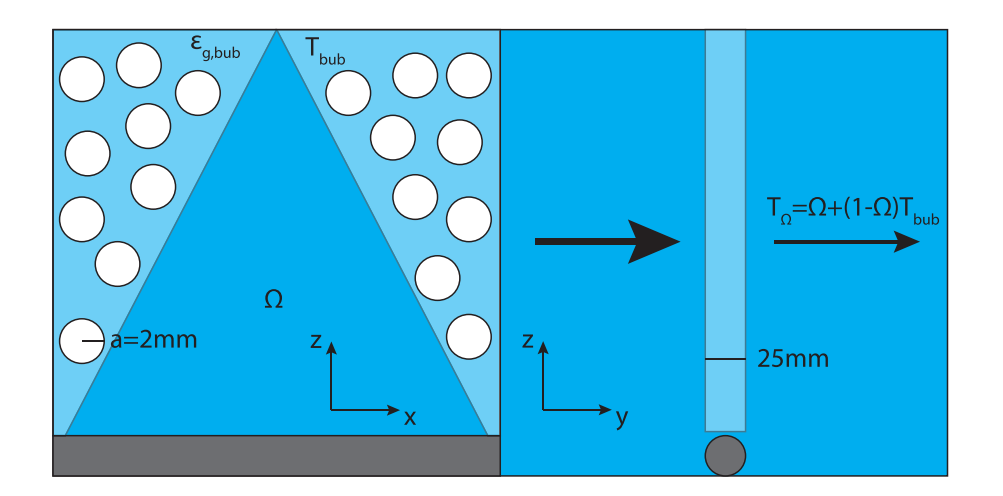


FIG. 10. Schematic overview of the structures close to the manifold.

and the deformation along the length of the manifold (e.g., Beelen et al., 2023). All of these temporal variations contribute to the spread in the IL. The cloud-like structure in particular, has a known effect on the transmission of sound waves (e.g., d'Agostino and Brennen, 1988; Kozhevnikova and Bjørnø, 1992; Omta, 1987) and changes in the structure can thus change the acoustic properties of the bubble curtain. Further variations in the structure of the curtain can have an effect on the sound transmission if the typical size of these structures is large as compared to the wavelength of a sound wave. Equivalent fluid models using an average description of the bubble curtain profiles will not be able to describe the fluctuations in the IL over time. The variations in the IL show that the actual distribution of the air in the bubble curtain is important. Furthermore, taking the average of the acoustic properties based on instantaneous void fraction distributions for many instances of a bubble curtain in time generally does not equal the acoustic properties based on the average void fraction distributions for the same instances of the bubble curtain. The bubble curtain representation using the average void fraction distribution could, therefore, lead to inaccurate acoustic predictions. It is currently unknown how variations in the instantaneous distributions describing the bubble curtain affect the acoustic performance of the bubble curtain as compared to the performance of a theoretical bubble curtain with the average void fraction distribution. For instances of the bubble curtain featuring a larger number of holes, the performance will

likely deteriorate. On the other hand, if at the same time bubble clouds respond to a more desirable frequency, it might improve the relevant performance.

Another shortcoming of the acoustic models, as they are currently used, is related to equivalent fluid modelling. Experiments aimed at solely measuring the response of a typical bubbly mixture for bubble curtains (gas fraction on the order of $\sim 1\%$ and bubble radii on the order of $\sim 2 \text{ mm}$) to sound have not been carried out. Commander and Prosperetti (1989) mention that their model is not applicable in the ranges that it is currently used for in bubble curtains. We would like to shortly discuss a concept for measuring the isolated bubble plume response to sound, since the lack of validation data remains problematic. If a hydrophone is placed inside a bubble plume (i.e., inside the bubbly mixture) while keeping the source outside this plume, likely all sound sources other than the sound generated by the hydrosounder or airgun are negligible. Since the hydrophone is inside the bubble plume, it is as much shielded from the background noise, the noise generated by the bubble generation, and the indirect sound paths as it is from the direct sound. Since the direct sound is significantly louder than the other sounds, they can be neglected. This is assuming the sound generated by the bubble plume stems from the manifold and the water surface, not from the rising of the bubbles itself. By measuring inside the bubble plume, one could get more insight on the isolated response of the bubble curtain to the generated sound. Moreover, it can be incorporated in

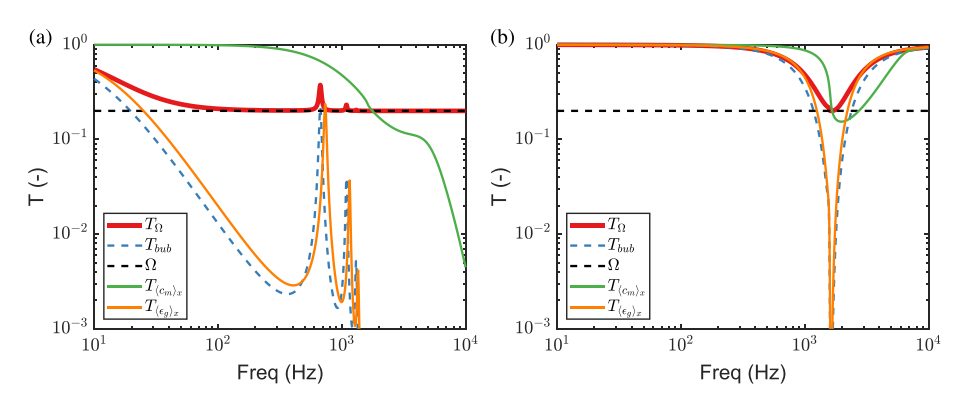


FIG. 11. Transmission coefficient based on different approaches of calculating the speed of sound. (a) $\epsilon_{g,bub} = 0.1$, (b) $\epsilon_{g,bub} = 0.001$.

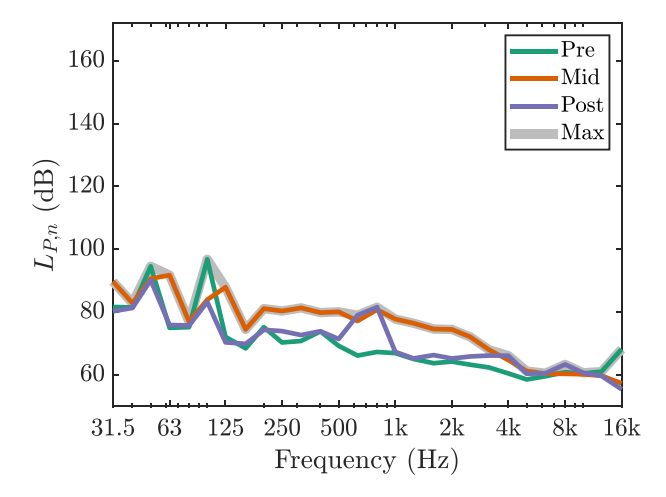


FIG. 12. Background noise levels measured at the fourth receiver location at three different time instances.

experiments such as the ones explained in this paper by moving one of the hydrophones to within the bubbly mixture.

D. Holes in the bubble curtain

From the theoretical considerations and from the model results, it seems that voids in the bubble distribution are likely an important factor for the characterization of bubble curtains. Holes in the bubble curtain can be considered as sources of sound leakage. Close to the manifold, the presence of holes is most obvious. Representing these holes as a region with the speed of sound of water in our 2.5D FE model brings the modelled results closer to the measured results (see Fig. 5). The simulation with the gap shows that the relatively small gap transmits more sound than the rest of the bubble curtain. A more thorough study, including experiments and modelling, is needed to investigate the role of openings in the curtain in more detail.

In this context, it is also noteworthy to consider the results of Rustemeier *et al.* (2012) who reported a significantly improved performance for a bubble curtain emanating from a membrane instead of individual nozzles. These authors named the reduced bubble size as a potential reason for the increased IL when using the membrane. However, this effect could not explain the full

performance improvement observed in the experiments. It therefore appears plausible and likely that the transparency, which is greatly reduced when using the membrane, also is a relevant factor here.

The cloud-like structure in a developed bubble curtain could lead to local holes in the bubble curtain, temporarily increasing the transparency. This could partially explain the variability in the performance of the bubble curtain between different shots of the air gun [see Fig. 7(d)].

Finally, even if the gap is included in the model, the model results retain a flow rate dependence at lower frequencies. This is not seen in the experimental data. Interestingly, the experimentally observed flow rate dependence of the IL between the flowrates 36 and 96 Lmin⁻¹ [see Fig. 7(a)] is actually not seen for the model including the gap. Note, however, that the size of the gap in the model is not dependent on flow rate. It therefore appears possible that larger effective openings were present at those lowest flow rates (e.g., not all nozzles operating or reduced lateral mixing), reducing the IL for these cases.

VII. CONCLUSION AND OUTLOOK

In this paper, we have investigated the impact of the configuration of bubble curtain(s) on the IL based on measurements and on modelling. The experiments show that splitting the air flow rate into two distinct bubble curtains significantly increases the IL for frequencies exceeding 100-500 Hz, which is relevant for pile driving. Similarly, the modelling indicates a significant improvement when splitting up the air flow rate. The distance between the bubble curtains will influence the frequency range in which splitting up the air flow rate over two manifolds is effective. We attribute the improvement in IL when splitting up the air flow rate to the introduction of a secondary reflective boundary without compromising the effectiveness of the individual curtains too much, since the speed of sound increases only marginally due to the reduction in flow rate per curtain. This study shows there is room for improvement in the performance of bubble curtains without increasing the net air flow rate when considering the configuration as part of the optimization strategy. These benefits need, of course, to be weighed against the cost of installing an additional bubble curtain. For single bubble curtains, our results show that

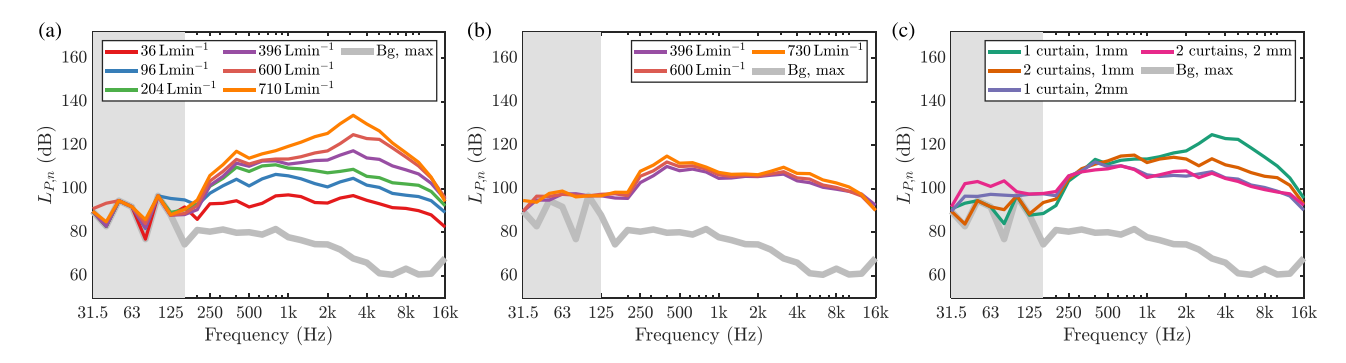
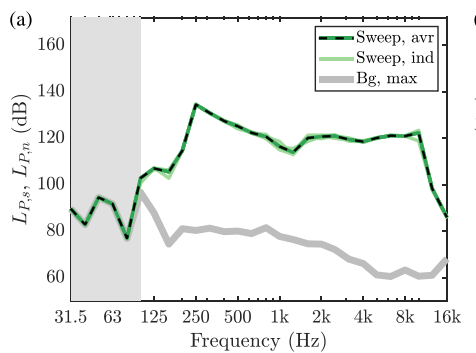


FIG. 13. Recorded sound from the bubble curtains for different flow rates. (a) With 1 mm nozzles, (b) with 2 mm nozzles, (c) comparison between the sound generated by different configurations at $600 \, \mathrm{Lmin}^{-1}$.



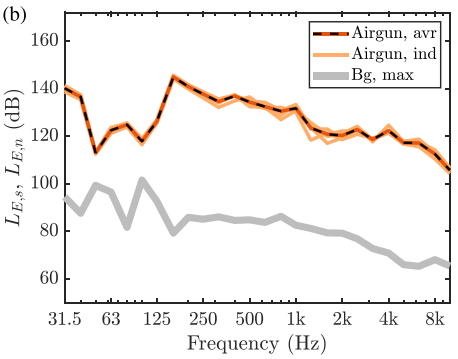


FIG. 14. (a) Sound generated by the J11 hydro sounder measured by the fourth receiver, (b) sound generated by the TNO's mini airgun measured by the fourth receiver.

using lower air flow rates may have only a limited impact on the performance.

In addition to these findings regarding the performance of the considered air curtain configurations, a number of other insights are noteworthy. We have seen that the IL does not depend on the flow rate in our measurements, whereas it does when considering the model results using the average void fraction to compute the effective speed of sound. We did obtain a flow rate independent result for higher frequencies when we consider the presence of an opening (e.g., close to the nozzles) in the modelled bubble curtain. This finding requires further investigation. The effectiveness of the gap indicates its importance; however, we want to stress that this finding does not mean that this was the missing part in the further correct modelling. The effectiveness of the gap can also disguise the fact that the equivalent fluid models currently employed may not be suitable for the considered conditions (i.e., void fraction range and frequencies close to or at bubble resonance).

Another issue that deserves further investigation is the effect of using the average void fraction distribution to calculate the acoustic properties instead of using multiple instances of the instantaneous void fraction distribution to calculate the acoustic response and average over that. To accurately capture the details of the bubble curtain structure that exist at each instance and its effect on the acoustic performance, 3D simulations would be required. However, 2D simulations, including variations in the bubble curtain in the direction perpendicular to the manifold, could also already provide important insight in its effect.

For many of the higher air flow rates, a louder sound source would be required to increase the frequency range in which the measured signals are above the noise floor and the IL can correctly be assessed. At the same time, the indirect paths of the sound should be limited as much as possible so that experimental results in basins can be translated more easily to real-life applications. The latter might be impossible in a basin such as the one used for our experiments. To isolate the effect of a bubble curtain, from its surrounding, we suggested in Sec. VIC to place a hydrophone inside a bubble curtain. These experiments could function as a benchmark case for acoustic modelling of bubble plumes. Obviously, these acoustic measurements should be accompanied by hydrodynamic measurements of the void fraction and bubble size distribution.

Further research in applying two bubble curtains, using the same air flow rate, for full scale applications should also be carried out. For example, our finding implies that halving the air flow rate per curtain benefits the overall IL, but this only works if the bubble curtains remain continuous. The potential for up-scaling this approach should therefore be carefully investigated.

ACKNOWLEDGMENTS

We gratefully acknowledge the support by TNO and MARIN and, in particular, Frans Staats, Martijn van Rijsbergen, and Heerko Koops during the measurements. We would also like to thank Gert-Wim Bruggert and Thomas Zijlstra for their help in preparing the experimental setup.

AUTHOR DECLARATIONS Conflict of Interest

The authors have no conflicts to disclose.

DATA AVAILABILITY

The data used in this study are available from the corresponding author upon reasonable request.

APPENDIX A

In Fig. 8, we show the six logarithmic sweeps generated by the J11 hydrosounder per measurement. The frequency sweeps are linear against the logarithmic *y* axis as shown by the line (A). Along with the main signal, the source also generates higher harmonics as is evident from the parallel lines (B). The J11 also unintentionally generates lower frequencies (C). These higher and lower frequencies can sometimes be useful for analysis outside of the intended range although they do lack power. Finally, we see a slight lack in the synchronization (D) such that the sixth sweep is not entirely captured. We therefore use the first five sweeps.

APPENDIX B

In this appendix, we discuss details regarding the implementation of the model in COMSOL.

1. Domain

An overview of the modelled domain is given in Fig. 9. It consists of a pure water domain (blue in Fig. 9), two domains where the bubble curtains are positioned (cyan in Fig. 9) with accompanying transition domains (purple in Fig. 9), and on both ends, a so-called perfectly matched layer (PML). We will discuss the implementation of each domain in Appendixes Appendixes B 2 and B 3.

The location of the source is shown in red. The location of the source and receivers corresponds to the locations of the source and receivers in the experiments. The four receivers are shown by the green dots. The boundaries are defined by the PMLs (explained below) and by the bottom and water surface.

2. Bubble curtain

The complex valued equivalent sound speed of the bubble curtain $\langle c_m \rangle(y,z)$ is saved into a lookup table, which is interpolated to the Gauss integration points of the local mesh in the domain assigned for the bubble curtain.

3. PML

The PML was first introduced by Qi and Geers (1998) for acoustic problems. The PML is a non-physical material which is used as a boundary to a computational domain. This boundary compactly and efficiently describes the damping of unbounded media. In other words, the PML represents a long open domain in which the acoustic pressure is dampened. In COMSOL, a PML is readily implemented [see, e.g., Zampolli *et al.* (2008)] and has been applied for the currently presented model. As the name suggests, the PML retains the same properties as the material it is supposed to represent; this entails that, although there is a lot of damping, no reflections will result from this implementation.

4. Mesh

The mesh will be auto-generated by COMSOL, given some manual restrictions on the mesh size. For an accurate description of the solution, using quadratic elements, the mesh size ($s_{\rm mesh}$) needs to be smaller than a quarter of the smallest wavelength considered

$$s_{\text{mesh}} \le \frac{1}{4} \frac{c_m}{f_{\text{max}}} = \frac{1}{4} \lambda_{\text{min}}.$$
 (B1)

For the cases at hand, $f_{\rm max}=5495\,{\rm Hz}$ is the maximum frequency considered for the solution and $\lambda_{\rm min}$ is the accompanying minimum wavelength. In the water and PML domains, this condition has been implemented by $1/8\,\lambda_{\rm min}$ < $s_{\rm mesh}<1/4\,\lambda_{\rm min}$, with $\lambda_{\rm min}\approx0.27\,{\rm m}$. The mesh in the water domain is a rectangular mesh fulfilling the aforementioned condition for the smallest side of the rectangle. In practice, the mesh size is as large as possible while fitting well within the geometric constrictions of the domain, such that it is closer to $1/4\,\lambda_{\rm min}$.

In the bubble curtain domain, we also chose to employ a constant mesh size; for that, the minimum sound speed in the bubble curtain has to be set beforehand. However, the sound speed can locally be as low as $\langle c_{m,\min} \rangle \approx 20 \, \text{ms}^{-1}$, resulting in a very dense mesh. It must be noted that these very low sound speeds are only observed in very narrow parts of the center of the bubble curtain for specific frequencies and curtain configurations. To alleviate the condition on the mesh size [see Eq. (B1)], we experimentally tested with different effective minimum sound speeds, to find $\langle c_{m,\min} \rangle$ $= 75 \,\mathrm{ms}^{-1}$ to still faithfully describe the solution. The shortest wavelength considered and thus determining the mesh size is $\lambda_{min} \approx 13.6 \, mm$ and is more than sufficient for the vast majority of the bubble curtain domain. A further criterion on the mesh size is that it should be able to describe the local changes in the speed of sound accurately, which was experimentally found to be the case using the aforementioned mesh size. The mesh in the bubble curtain domain is a triangular mesh allowing for more freedom in the mesh generation; although not relevant for the present study, this is implemented to allow for the option of a non-rectangular shape of the bubble curtain domain.

Finally, the transition region connects both meshes by free triangulation. This allows for a smooth transition between both meshes, with mesh sizes between the two aforementioned mesh sizes.

5. Propagation modes

As mentioned before, a 2.5 D model does not simulate the third dimension using FE simulations but assumes a solution to the Helmholtz equation fitting the boundary conditions. For Cartesian coordinates, the solution to the one-dimensional (1D) Helmholtz equation satisfying acoustically hard boundary conditions takes the form of cosine functions. The excitation, which is a point excitation in the middle of the basin, is expanded into this set of cosine functions to obtain the contribution of each mode. The solution will only include the symmetric cosines, since these can be actuated by the source and fit within the symmetric domain. In the FE calculation, which is needed to obtain the *y-z* component of the solution, each mode uses an augmented wave number

$$k_a^2 = k_{y,z}^2 = k_{x,y,z}^2 - k_x^2.$$
 (B2)

The augmented wave number, k_a , or $k_{y,z}$, is used since we use a 2D simulation for a 3D problem. It is effectively the projection of the 3D wave number on the 2D plane (y, z-plane) (Cao and Greenhalgh, 1997; Novais and Santos, 2005). k_x is the wave number of the solution in the x-direction and $k_{x,y,z}$ is the local wave number of the fluid or mixture (c/ω) or c_m/ω , respectively, with $\omega = 2\pi f$). Since the source is placed in the center of the domain, only the even contributions of the cosines and a constant solution need to be taken into account. We have taken the first five even modes into account, leading to minimal truncation errors while maintaining a manageable computational effort. Equation (B2) indicates that for

large k_x , relative to the real part of $k_{x,y,z}$, the imaginary part of the augmented wave number, k_a , becomes dominant, yielding evanescent waves. The higher modes are thus generally dampened quickly and hardly contribute to the overall solution, especially at larger distances from the source. To retrieve the approximated 3D solution, the 2D solution, calculated using the augmented wave number, needs to be multiplied with the associated mode shape in the x-direction and then summed. However, since the receivers (the hydrophones) are, just like the source, placed in the symmetry plane, we can simply sum the 2D solutions of the different modes to find the solution in this plane.

6. Source

Since we represent the result in terms of the IL, the source representation is not a critical factor in the model, i.e., we are only interested in the sound reduction by the bubble curtain(s). In reality, the directionality of the source could, however, influence the measured IL. The source is implemented as a point source, since the source in the experiments is roughly omnidirectional. The coordinates of the source are x_s , y_s , and z_s and correspond to the locations of the source in the experiments.

7. Receivers

The solution is interpolated to the receiver locations to correspond to the locations of the hydrophones in the experiments. For these receiver points, the IL was calculated according to Eq. (1). The coordinates of the receivers are $x_{r,i}$, $y_{r,i}$, and $z_{r,i}$ with i = [1, 2, 3, 4].

8. Boundary conditions

At the water surface, the acoustic pressure vanishes, known as the pressure release condition or as the "sound soft boundary" in COMSOL. At the bottom of the tank and at the end of the PMLs, the normal component of the velocity vanishes, known as the "sound hard boundary" in COMSOL. The latter boundary condition approximates the walls of the basin; however, in practice, the impedance mismatch between the water and the basin walls is limited, meaning the sound can partially pass through the wall. This boundary condition thus omits the interaction between the water and the walls and soil and the secondary path this creates in practice.

APPENDIX C

In this appendix, we explore the effect of holes in a bubble curtain. Currently, these structures are generally not taken into account in the equivalent fluid modelling of bubble curtains. The equivalent fluid model usually assumes a homogeneous bubble distribution after which the equivalent speed of sound is calculated, which, in turn, is input to the 2.5 D simulation. In this appendix, we will discuss using the theory that is the basis to the equivalent fluid modelling, why disregarding holes in the bubble curtain could be

problematic, and what is the best (or least bad) option for calculating the effective speed of sound in the presence of these holes.

Bubble curtains are typically generated from an array of individual round plumes, which eventually merge to form a continuous quasi-2D bubble plume. This leads to an inhomogeneous distribution of the void fraction in the region close to the nozzles, which is also reflected in the hydrodynamic model used to calculate the void fraction and bubble size distributions. This variation in the void fraction along the *x*-direction, in turn, leads to a variation of the speed of sound in the same direction. The reduction to an effective speed of sound required for the 2D model can then be achieved in multiple ways, of which we take the two most common, namely,

$$c_{eff} = \langle c_m \rangle_x(y, z)$$
 (C1)

or,

$$c_{eff} = c_m(\langle \epsilon_g \rangle_x, y, z),$$
 (C2)

where $\langle \cdots \rangle_x = 2/\Delta x_n \int_0^{\Delta x_n/2} \cdots dx$ denotes the spatial average in the *x*-direction. That is, we can either calculate the speed of sound first and then average [Eq. (C1)] or determine the average void fraction first and then calculate the speed of sound [Eq. (C2)]. The described order of averaging is important due to the non-linear relationship between the void fraction and the speed of sound, currently the latter [Eq. (C2) is mostly used]. The 2D model aims at representing the actual 3D situation, implying that the effective speed of sound needs to result in the correct transmission of the sound pressure through the bubble curtain(s). We will evaluate the choice for the effective speed of sound based on a simplified theoretical situation sketched in Fig. 10, which approximates the void fraction distribution close to the nozzles.

For the proposed simplified analysis, we assume the bubble curtain to consist of a homogeneous bubbly regime and a pure water regime. In this way, we can compare the transmission resulting from our choice of the speed of sound to the theoretical result. The transparency factor Ω denotes the fraction of the cross section in the x-z plane which does not contain bubbles. We assume that there is no transmission loss in the region without bubbles, proportional to Ω , such that the power based transmission coefficient, T = 1, in this region. For the remaining surface, proportional to $1 - \Omega$, we adopt the transmission coefficient, T_{bub} , given by Commander and Prosperetti (1989) for the theoretical reference case. Note that this is an approximation since Commander and Prosperetti (1989) corresponds to the transmission coefficient of a homogeneously filled bubbly screen. The total theoretical transmission coefficient, T_{Ω} , is then given by the weighted average

$$T_{\Omega} = \Omega + (1 - \Omega)T_{bub},\tag{C3}$$

which results in $T_{\Omega} \to \Omega$ in the limit $T_{bub} \to 0$. We now compare the resulting transmission coefficient of Eq. (C3) with two alternative estimates, viz. a transmission

coefficient based on a space averaged sound speed $(T_{\langle c_m \rangle_x})$ according to Eq. (C1) and a transmission coefficient based on an averaged void fraction $(T_{\langle \epsilon_g \rangle_x})$, according to Eq. (C2). In Fig. 11, the resulting transmission coefficients are shown.

We use a relatively high void fraction in Fig. 11(a) in the bubble regime of $\epsilon_{g,bub}=0.1$ due to the fact that the structures resulting from the hydrodynamical model occur only close to the manifold where the void fraction is high. In practice, however, holes can also occur as a result of the structures due to the cloud-like behaviour of the bubbles or as a result of currents at sea. Therefore, we also show a low void fraction in Fig. 11(b). In this way, we can roughly estimate the impact of holes higher up in the bubble curtain. We use a homogeneous bubble size distribution with a bubble radius of a=2 mm, a transparency factor of $\Omega=0.2$, and a thickness of 25 mm (based on 1/4 of the inter-nozzle distance of the manifolds used in our experiments).

In particular, in Fig. 11(a), but also in Fig. 11(b), it can be seen that both transmission coefficients $(T_{\langle c_m \rangle_x})$ and $T_{\langle \epsilon_g \rangle_x}$ do not agree with the estimate in Eq. (C3). However, unlike $T_{\langle c_m \rangle_r}$, $T_{\langle \epsilon_g \rangle_r}$ is largely consistent with the behaviour of a homogeneous bubble curtain, (T_{bub}) , and also approximates T_{Ω} reasonably well at the lower void fraction. The better (or least bad) option is thus to first average the void fraction and then calculate the speed of sound. An additional benefit of this approach is that it will likely be able to represent the socalled wall effect more closely. The wall effect was first discussed by Korteweg (1878) and Moens (1877). They found that the pressure pulse in blood vessels did not move with the higher speed of sound in the blood but rather with a lower speed of sound, depending on the properties of the blood vessel (the wall). In this analogy, the bubble plume acts as the blood vessel and the pure water as the blood. The speed of sound through the holes should then be lower than that of water. This effect would thus favor the void fraction averaged result; the openings, however, cannot be considered narrow everywhere such that the importance of this effect could be minimal.

A further observation in relation to Fig. 11 is that potential positive effects through increasing the void fraction or changing the bubble size distribution are largely cancelled out by the effect of the holes in the bubble curtain. The minimal transmission coefficient is namely limited by Ω . This is similar to a door that is ajar, where the total transmission is determined by the opening such that improving the structure has no effect. The door can be seen as the bubble curtain with the transmission coefficient, T_{bub} , and the fact that it is ajar as the holes, represented by Ω . In that case, the fact that it is ajar sets a lower limit to the relevance of the effectiveness of the door. Following this argumentation leads to a flow rate independent IL if the holes are important. However, the environment of the hole (the impedance of the bubble curtain surrounding it) affects the IL. See also the discussion of the "slit on the ground" in Wang et al. (2023).

One possible way of dealing with the inability to find a proper effective speed of sound can be to translate the 3D holes to a 2D gap. In other words, replace part of the bubble

curtain by pure water, similar to Peng *et al.* (2021). However, translating the 3D holes to a 2D gap is non-trivial, for example, due to the before mentioned wall effects. Also, the interaction between the holes and the frequency of the incident sound wave is largely unknown.

APPENDIX D

We measured the background noise three times, as mentioned in Sec. III. In Fig. 12, the background levels recorded at the fourth receiver are shown as recorded before the measurements (Pre), between the measurements with the J11 and the airgun (Mid), and after all measurements had been concluded (Post). The background noise level, which we will show in the figures, is the maximum of the measured signals (shown in gray in Fig. 12). The background measurements are similar for all receivers (not shown); however, due to the larger distance from the source, the recorded signal levels are lower and the background level of the fourth receiver will be most limiting.

APPENDIX E

The bubble curtains generate noise themselves. We measured the generated sound for the different configurations we use. In Fig. 13(a), it is shown that the generated sound levels by one manifold with 1 mm nozzles is highly air flow rate dependent. Particularly at higher frequencies, the SPL increases with increasing air flow rate. For one manifold with 2 mm nozzles, we only investigated the higher air flow rates, and found no clear flow rate dependency [see Fig. 13(b)]. In Fig. 13(c), it is clear that two bubble curtains generated by 1 mm nozzles generate less sound than one with the same total air flow rate. The main reason being the halved air flow rate per manifold [see Fig. 13(a)] and the fact that the noise produced by the first manifold is shielded by the bubble curtain emitting from the second manifold. We see that the 2 mm nozzles generate generally less noise at higher frequencies (>250 Hz) compared to the 1 mm nozzles, but do the opposite at lower frequencies $(<250\,\mathrm{Hz}).$

The sound generated by the bubble curtains is well above the background noise levels in the region of interest. This implies that the sound level by the bubble curtains can now be considered the background noise level for the measurements taken with a bubble curtain active. These lines are therefore generally shown instead of the background noise levels. We furthermore present the 2 mm nozzle results if possible due to the slightly lower sound levels in the region of interest.

APPENDIX F

The J11 hydro sounder is actuated by logarithmic sweeps in a range of 0.1–10 kHz; however, the source generates additional, unintended, harmonics which can also be used in our analysis. For measuring the IL, having

harmonics is not a problem; as long as the signal-to-noise ratio is sufficient, it can be used. If the total noise level is less than 3 dB above the background noise level, the source level can no longer be considered distinguishable; for that reason, we disregard this part of the measurement [see the gray area and the dashed line in Fig. 14(a). We plot both the individual sweep results and the averaged result, showing that the signal is well reproducible. The mini airgun generates, mainly at the lower frequencies, a significantly higher sound level. At higher frequencies, the signal generated by the airgun becomes less constant between different instances. Above 10 kHz, we stop the analysis since the source level is limited and the spread in the signal yields unreliable results.

APPENDIX G

In this appendix, we focus on estimating the contribution of the temporal variations in the plume on the variation in the IL. This requires the exclusion of the variation due to the airgun.

If we consider the following relation for the SEL at the fourth receiver based on the SEL at the first receiver without a bubble curtain

$$SEL_{nc,4} = SEL_{nc,1} - \Delta SEL_{nc,1\to 4}, \tag{G1}$$

with $\Delta SEL_{nc,1\rightarrow4}$ being the difference in SEL between both locations without an active bubble curtain. We can further write the SEL at the first receiver without a bubble curtain as

$$SEL_{nc,1} = SEL_{c,1} - \Delta SEL_{c-nc,1}.$$
 (G2)

The IL at the fourth receiver, based on Eqs. (G1) and (G2), is given by

$$\begin{split} \text{IL}_4 &= \text{SEL}_{nc,4} - \text{SEL}_{c,4} \\ &= \text{SEL}_{c,1} - \Delta \text{SEL}_{c-nc,1} - \Delta \text{SEL}_{nc,1\to4} - \text{SEL}_{c,4}. \end{split} \tag{G3}$$

Splitting IL₄ up into its components allows us to discuss the origin of the variations in IL₄. Variations in $\Delta SEL_{nc,1\rightarrow4}$ do not depend on the variations in the bubble curtain. The variations in this parameter are assumed to be very limited since the path of transmission does not change. In other words, if we were to measure this variable, we would measure the difference in SEL at receiver 1 and 4 without a bubble curtain present and we expect that to be very reproducible.

Variations in $\Delta SEL_{c-nc,1}$ are likely significant and likely stem from temporal variations in the (first) bubble curtain. The reflecting sound on the (first) bubble curtain is known to impact the measured SEL at the first receiver [see Fig. 3(a)], and the level of the reflected sound likely depends on the instantaneous bubble distribution.

So, the variations in $SEL_{c,1} - SEL_{c,4}$ are likely due to the temporal variations of the bubble curtain and related to the variations in IL₄. However, we have now replaced the

uncertainty of the variations in the source level with the uncertainty of the variations in $\Delta SEL_{c-nc,1}$. The benefit of this approach is that the variations in the IL now only depend on the instantaneous state of the bubble curtain since these values are measured using the same instance of the source level.

Bailey, H., Senior, B., Simmons, D., Rusin, J., Picken, G., and Thompson, P. M. (2010). "Assessing underwater noise levels during pile-driving at an offshore windfarm and its potential effects on marine mammals," Mar. Pollut. Bull. 60(6), 888–897.

Beelen, S., and Krug, D. (2024). "Planar bubble plumes from an array of nozzles: Measurements and modelling," Int. J. Multiph. Flow 174, 104752.

Beelen, S., van Rijsbergen, M., Birvalski, M., Bloemhof, F., and Krug, D. (2023). "In situ measurements of void fractions and bubble size distributions in bubble curtains," Exp. Fluids 64(2), 31.

Bellmann, M. A. (2014). "Overview of existing noise mitigation systems for reducing pile-driving noise," in *Proc. auf der Internoise*.

Cao, S., and Greenhalgh, S. (1997). "2.5-D acoustic wave modelling in the frequency-wavenumber domain," Explor. Geophys. 28(2), 11–15.

Carstensen, E., and Foldy, L. (1947). "Propagation of sound through a liquid containing bubbles," J. Acoust. Soc. Am. 19(3), 481–501.

Chmelnizkij, A., von Estorff, O., Grabe, J., Heins, E., Heitmann, K., Lippert, S., Lippert, T., Ruhnau, M., Siegl, K., Bohne, T., Grießmann, T., Rolfes, R., Rustemeier, J., Podolski, C., Rabbel, W., and Wilken, D. (2016). "Schlussbericht des verbundprojektes bora: Entwicklung eines berechnungsmodells zur vorhersage des unterwasserschalls bei rammarbeiten zur gründung von owea" ("Final report of the bora joint project: Development of a calculation model to predict underwater noise during ramming work for the founding of owea"), Technische Universität Hamburg-Harburg, Leibniz Universität Hannover, Christian-Albrechts-Universität zu, Kiel, Hamburg, Hannover & Kiel.

Commander, K. W., and Prosperetti, A. (1989). "Linear pressure waves in bubbly liquids: Comparison between theory and experiments," J. Acoust. Soc. Am. 85(2), 732–746.

Dahl, P. H., de Jong, C. A., and Popper, A. N. (2015). "The underwater sound field from impact pile driving and its potential effects on marine life," Acoust. Today 11(2), 18–25.

Dähne, M., Tougaard, J., Carstensen, J., Rose, A., and Nabe-Nielsen, J. (2017). "Bubble curtains attenuate noise from offshore wind farm construction and reduce temporary habitat loss for harbour porpoises," Mar. Ecol. Prog. Ser. 580, 221–237.

d'Agostino, L., and Brennen, C. E. (1988). "Acoustical absorption and scattering cross sections of spherical bubble clouds," J. Acoust. Soc. Am. 84(6), 2126–2134.

Domenico, S. (1982). "Acoustic wave propagation in air-bubble curtains in water—Part I: History and theory," Geophysics 47(3), 345–353.

Feuillade, C. (1996). "The attenuation and dispersion of sound in water containing multiply interacting air bubbles," J. Acoust. Soc. Am. 99(6), 3412–3430.

Guo, Y., Wang, H., and Lian, J. (2022). "Review of integrated installation technologies for offshore wind turbines: Current progress and future development trends," Energy Convers. Manage. 255, 115319.

Hastie, G., Merchant, N. D., Götz, T., Russell, D. J., Thompson, P., and Janik, V. M. (2019). "Effects of impulsive noise on marine mammals: Investigating range-dependent risk," Ecol. Appl. 29(5), e01906.

Igoe, D., Gavin, K., and O'Kelly, B. (2013). "An investigation into the use of push-in pile foundations by the offshore wind sector," Int. J. Environ. Stud. 70(5), 777–791.

J11 hydrosounder (2024). https://www.navsea.navy.mil/Home/Warfare-Centers/NUWC-Newport/What-We-Do/Detachments/Underwater-Sound-Reference-Division/Transducer-Standards/Transducer-Catalog (Last viewed October 9, 2024).

Juretzek, C., Schmidt, B., and Boethling, M. (2021). "Turning scientific knowledge into regulation: Effective measures for noise mitigation of pile driving," J. Mar. Sci. Eng. 9(8), 819.

Korteweg, D. J. (1878). "Ueber die fortpflanzungsgeschwindigkeit des schalles in elastischen röhren" ("On the propagation speed of sound in elastic tubes"), Ann. Phys. 241(12), 525–542.

https://doi.org/10.1121/10.0035817

- Kozhevnikova, I., and Bjørnø, L. (1992). "Experimental study of acoustical emission from bubble cloud excitation," Ultrasonics 30(1), 21–25.
- Lippert, S., Nijhof, M., Lippert, T., Wilkes, D., Gavrilov, A., Heitmann, K., Ruhnau, M., von Estorff, O., Schäfke, A., Schäfer, I., Erlich, J., MacGillivray, A., Park, J., Seong, W., Ainslie, M., de Jong, C., Wood, M., Wang, L., and Theobald, P. (2016). "COMPILE—A generic benchmark case for predictions of marine pile-driving noise," IEEE J. Ocean. Eng. 41(4), 1061–1071.
- Merchant, N. D. (2019). "Underwater noise abatement: Economic factors and policy options," Environ. Sci. Policy 92, 116–123.
- Moens, A. I. (1877). Over de Voortplantingssnelheid Van Den Pols (On the Speed of Propagation of the Pulse) (SC Van Doesburgh, Leiden, The Netherlands).
- Musial, W. D., Beiter, P. C., Spitsen, P., Nunemaker, J., and Gevorgian, V. (2019). 2018 Offshore Wind Technologies Market Report, Technical Report (U.S. Department of Energy Office of Scientific and Technical Information, Oak Ridge, TN).
- Nehls, G., Rose, A., Diederichs, A., Bellmann, M., and Pehlke, H. (2016). "Noise mitigation during pile driving efficiently reduces disturbance of marine mammals," in *The Effects of Noise on Aquatic Life II* (Springer, Berlin), pp. 755–762.
- Novais, A., and Santos, L. T. (2005). "2.5 D finite-difference solution of the acoustic wave equation," Geophys. Prospect. 53(4), 523–531.
- Omta, R. (1987). "Oscillations of a cloud of bubbles of small and not so small amplitude," J. Acoust. Soc. Am. 82(3), 1018–1033.
- Peng, Y., Tsouvalas, A., Stampoultzoglou, T., and Metrikine, A. (2021). "Study of the sound escape with the use of an air bubble curtain in off-shore pile driving," J. Mar. Sci. Eng. 9(2), 232.
- Popper, A. N., Hice-Dunton, L., Jenkins, E., Higgs, D. M., Krebs, J., Mooney, A., Rice, A., Roberts, L., Thomsen, F., Vigness-Raposa, K., Zeddies, D., and Williams, K. A. (2022). "Offshore wind energy development: Research priorities for sound and vibration effects on fishes and aquatic invertebrates," J. Acoust. Soc. Am. 151(1), 205–215.
- Qi, Q., and Geers, T. L. (1998). "Evaluation of the perfectly matched layer for computational acoustics," J. Comput. Phys. 139(1), 166–183.
- Rustemeier, J., Grießmann, T., and Rolfes, R. (2012). "Underwater sound mitigation of bubble curtains with different bubble size distributions," Proc. Mtgs. Acoust. 17, 070055.
- Spagnoli, G., and Weixler, L. (2013). "New technologies for offshore piles installation," in *Offshore Mediterranean Conference and Exhibition* (OMC, Ravenna Italy), pp. OMC–2013.

- Stein, P., Sychla, H., Gattermann, J., and Degenhardt, J. (2015). "Hydro sound emissions during impact driving of monopiles using hydro sound dampers and big bubble curtain," in *RAVE Offshore Wind R&D Conference*, Bremerhaven, German.
- Stöber, U., and Thomsen, F. (2019). "Effect of impact pile driving noise on marine mammals: A comparison of different noise exposure criteria," J. Acoust. Soc. Am. 145(5), 3252–3259.
- Strietman, W., Michels, R., and Leemans, E. (2018). 2018-087 Measures to Reduce Underwater Noise and Beach Litter: An Assessment of Potential Additional Measures for The Netherlands (Wageningen Economic Research, Wageningen, the Netherlands).
- The European Marine Observation and Data Network (2023). https://emodnet.ec.europa.eu/geoviewer/#!/ (Last viewed December 12, 2023).
- Tougaard, J., and Dähne, M. (2017). "Why is auditory frequency weighting so important in regulation of underwater noise?," J. Acoust. Soc. Am. 142(4), EL415–EL420.
- Tsouvalas, A. (2020). "Underwater noise emission due to offshore pile installation: A review," Energies 13(12), 3037.
- von Pein, J., Lippert, T., Lippert, S., and von Estorff, O. (2022). "Scaling laws for unmitigated pile driving: Dependence of underwater noise on strike energy, pile diameter, ram weight, and water depth," Appl. Acoust. 198, 108986.
- Wang, B., Lai, C. C., and Socolofsky, S. A. (2019). "Mean velocity, spreading and entrainment characteristics of weak bubble plumes in unstratified and stationary water," J. Fluid Mech. 874, 102–130.
- Wang, C., Utsunomiya, T., Wee, S., and Choo, Y. (2010). "Research on floating wind turbines: A literature survey," IES J. Part A: Civil Struct. Eng. 3(4), 267–277.
- Wang, S., Yang, Z., Tao, J., Qiu, X., and Burnett, I. S. (2023).
 "Transmission loss and directivity of sound transmitted through a slit on ground," J. Acoust. Soc. Am. 153(1), 224–235.
- Wijngaarden, L. V. (1972). "One-dimensional flow of liquids containing small gas bubbles," Annu. Rev. Fluid Mech. 4(1), 369–396.
- Wood, A. B., and Lindsay, R. (1956). "A textbook of sound."
- Zampolli, M., Malm, N., and Tesei, A. (2008). "Improved perfectly matched layers for acoustic radiation and scattering problems," in *Proceedings of the COMSOL Conference*, Hannover, Germany.
- Zhu, S., Ooi, A., Skvortsov, A., and Manasseh, R. (2023). "Modelling underwater noise mitigation of a bubble curtain using a coupled-oscillator model," J. Sound Vib. 567, 117903.